NCBI Bookshelf. A service of the National Library of Medicine, National Institutes of Health.

Michael AC, Borland LM, editors. Electrochemical Methods for Neuroscience. Boca Raton (FL): CRC Press/Taylor & Francis; 2007.

Chapter 18 Principles, Development and Applications of Self-Referencing Electrochemical Microelectrodes to the Determination of Fluxes at Cell Membranes

Authors

Peter J. S. Smith, Richard H. Sanger, and Mark A. Messerli.

Introduction

The complexity of the neural microenvironment leads to two inevitable conclusions—in vivo studies are difficult and reduced preparations are simplistic. However, studying the brain environment and cellular function from both angles provides information that clearly advances our understanding of cellular function, signal processing, and diseased states. Implanted sensors in whole brain, both electrical and electrochemical, have contributed to our knowledge of Central Nervous System (CNS) organization and function. Recent moves to merge techniques of on-line capillary electrophoresis and detection of multiple chemicals simultaneously are exciting advances in understanding the CNS microenvironment [1]. Clearly, the chemical composition of this environment is important in not just sustaining the cells of the nervous system, but also in providing and controlling information transfer between neurons, glia and others. In vivo, however, studies are usually restricted to populations of cells and specific mechanisms are difficult to examine on a cell-by-cell basis. Reduced preparations and single cell studies offer insights into mechanisms, even if integration has been largely lost.

Tremendous advances in the approach to single cell studies has occurred in the past two decades. Electrophysiology has been dominated by the powerful derivatives of the original patch clamp technique, addressing the biophysics of single channels or whole cells [2]. Imaging has advanced our understanding of architectural dynamics and intracellular ion activities [3,4]. Indeed, the success of the latter displaced the use of intracellular, chemically-selective electrodes where voltage changes and competing ions make the technique difficult and the interpretation complex. Despite these limitations, electrochemical sensors have continued to demonstrate strength and versatility when applied to the external boundary layers of single cells and tissues. For example, Travis and Wightman [5] demonstrated a correlation between vesicle fusion and cell capacitance for dopamine release. In addition, scientists used electrochemistry of 5-HT and histamine to study quantal corelease [6]. Both of these examples require the placement of a carbon fiber, amperometric microelectrode, in close apposition to the plasma membrane where strong electrochemical signals can be derived over low background. These cases are special in that a discrete cellular event carries a clear electrochemically detectable, phasic, signal into the boundary layer. However, all cells modify the diffusive boundary layers because of physiology, for example transporter activities or respiration. These signals can be weak and often imposed on top of significant background levels of the same chemical–oxygen and calcium flux detection are examples. Problems in measuring changes of such chemical signals are further compounded by the instability of any electrode design. How can these limitations be overcome to make boundary layer measurements with high temporal and spatial fidelity?

This chapter proposes two approaches to making measurements in the boundary layer. Firstly, the gradient can be constrained by a restrictive space, effectively “amplifying” and defining the signal to be detected. Secondly, detection can be coupled directly to the chemical gradients radiating into or out of the cell. Two elegant examples of the first approach are available. Poitry et al. sought to measure the oxygen consumption and nucleotide levels, under closely matching conditions, for single cells [7]. To acquire the oxygen levels, they captured single rod photoreceptorsin glass micropipettes such that they lodged approximately 10 μm from the tip. Next, they inserted a Whalen-style oxygen electrode [8] through the pipette tip and measured oxygen consumption in a static configuration. Kang and Hilgemann [9] recently published results from a similar approach, but for the study of the Na^+ /Ca^{2+} exchanger in a cardiac muscle macropatch. Here an ion-selective electrode (ISE) was advanced into the body of a pipette supporting the macropatch. As the pipette geometry could be precisely modeled, Kang and Hilgemann were able to derive the stochiometry of this electroneutral transporter [9].

Coupling directly to the diffusive boundary layer, by alternating the placement of a chemically selective microelectrode in the proximity of active tissues or cells, was first reported by Gow et al. [10]. These investigators monitored pH changes proximal to a growing fungal hypha. The process of microelectrode placement and modulation was automated by Jaffe and Levy and applied to biological preparations by Kühtreiber and Jaffe [11,12]. In a more recent study, Kang et al. made measurements of the transmembrane potassium transport by “self-referencing” through movement of the macropatch relative to a K^+ ISE [13]. The development of this “self-referencing” technique, defined below, has occurred primarily at the BioCurrents Research Center, funded as a national resource by the National Institutes of Health (NIH:NCRR) since 1996, but also in other laboratories [14]. Smith et al. [15] coined the term “self-referencing” as it applies to this technique.

In the context of the electrochemical technique reviewed here, self-referencing refers to a modulation approach. The method belongs to a family of techniques employing temporal and time dependent, positional modulation of microprobes to enhance signal detection. Variants can be seen in scanning electrochemical microscopy, atomic force microscopy, and scanning reference electrode techniques used in both biological and materials science [16–19]. In the application described here, the term implies that a single sensor is modulated such that signal values obtained at the near pole (closest to the tissue or cell) can be compared to the values at the far pole (a known distance away). As will be discussed below, this delivers significant advantages in signal analysis with background, drift, and noise reduction—the electrode signal is effectively compared to itself at two locations. A second and independent reference electrode is also included to complete the circuit.

When positioned in a chemical gradient surrounding a single cell, or tissue surface, this type of electrochemistry generates a differential output that can be converted to a flux value through calibration and Fick's First Law. Using this approach with potentiometric electrodes, differential signals of low μvolts can be observed and with amperometric electrodes values of femtoamps are measured. The technique can be coupled with electrooptical and positional methods [20,21]. Overall, self-referencing of an electrochemical sensor offers the advantage of low signal detection, observation of non-electrogenic transport, use of ion-selective and redox based reactions, and enzymeassisted flux detection, all at the single cell level.

Self-Referencing: Principles

Cells modify the immediate chemical composition of the medium surrounding them. This is an inevitable consequence of physiologically driven molecular movements, both active and passive. For example, as a cell respires oxygen will be taken up from the medium and a shallow depletion gradient will exist around the plasma membrane, particularly in locations where mitochondria are localized [22]. Similarly the opening of a channel, or the activity of a pump, will locally modify the chemical concentrations/activities in a regional manner (Figure 18.1). These gradients reveal aspects of cell physiology in both normal and diseased states, making it of interest to couple to the gradients and thus gain insight into cell function. To measure a gradient, one needs two points of reference, a known distance apart, recording an identifiable analyte, with a known diffusion coefficient.

In a static configuration, drift, sensitivity, and chemical selectivity, or the lack of it, can have complicated implications for the use of these sensors, whether potentiometric or amperometric. In a self-referencing, non-invasive, mode of operation, many of these conventional problems can have a minimal impact, although other aspects influence the quantification of data recovered. The purpose of this paper is to highlight both the strengths and weaknesses of the self-referencing methodology.

The basic operational configuration of a self-referencing electrode is shown in Figure 18.2, where a calcium ISE is illustrated near a pipette source of calcium forming a defined gradient in the bulk solution (for details of this procedure and comparisons to modeled gradients see Smith et al. [15]). The ISE is moved in a square wave between two points in the gradient, usually 10 μm apart. This distance can be varied. The frequency of movement is usually 0.3 Hz. At that frequency, the electrode comes to rest for approximately 1 s at each pole after translation. As with distance, frequency can be independently controlled. The point nearest the source is referred to as the near-pole and the other as the far-pole. The convention is followed that if the electrode detects a higher concentration at the near-pole the flux is given a positive value indicating efflux. Signals are sampled 1000 times a second with the first 30% collected during and after translation being discarded. A final differential value is stored along with the correlated DC value, which can be compared to an original calibration slope.

The key to the sensitivity of this approach is that drift and background are relatively common to both positions of translation. Thus, the signal seen by the amplifiers when a calcium selective electrode is placed in a steep ion gradient, from an artificial source, may be similar to the result illustrated in Figure 18.3. No signal processing has taken place. A clear drift is seen in the signal from both poles of translation. Extracting a differential voltage or current, by subtracting the far pole signal from the near pole, minimizes the impact of drift and subtracts out background signals as well as contaminating voltages—such as junction potentials.

Although originally conceived for calcium flux detection [12,15,23], uses of ISEs for the detection of potassium and hydrogen [24] as well as chloride ion flux [25,26] have been popular extensions. Amperometric-based detection of nitric oxide (NO), oxygen, glucose and ascorbate, have proven powerful additional applications (references below and additional measurable analytes). No other approach permits repeated non-invasive observations on the same intact cell over hours or days, recording flux over periods of seconds, with a spatial resolution of a few microns. Figure 18.4 illustrates a Ca^{2+} ISE in the near pole of measurement next to an INS-1 cell. In this sense, the technique is unique, and complements other methods available to observe the movements of analytes across membranes or within cells.

Self-Referencing: Potentiometric Ion-Selective Electrodes (ISE)

Several recent studies have contributed to our understanding of the factors that influence ISE performance. Bakker et al. provide a review [27]. A key point they discuss is the importance of the internal electrolyte on detection limits, a matter dealt with below.

However, it is not the purpose of this paper to review methods of electrochemical detection so readers are referred to other reviews [27,28]. Here the researchers focus on the use of these designs in a self-referencing mode.

The ISEs are based on an ion-selective solvent or liquid membrane, immobilized in a silanized micropipette with tip diameters of 1–4 μm. For an ideal electrode the measured voltage, E , is related to the activity of the ion by the Nernst equation:

$$E = E_0 + S \log a_{\mathrm{i}} \tag{18.1}$$

where E_0 is an offset potential, S is the Nernstian slope

$$\frac{2.3RT}{z_{\mathrm{i}}F} \tag{18.2}$$

and a_{i} is the activity of the primary ion. R, T , and F have their usual meaning. The offset potential is composed of the boundary potentials and liquid junction potentials that exist across any circuit made up of a reference and measuring electrode. Through calibration of each ISE a value for the slope of the line, describing the voltage output and the change in ionic activity is collected. Since ionic activity is directly proportional to ion concentration, via the activity coefficient, and the changes that occur to this coefficient due to changes in ionic strength are usually negligible during self-referencing, we will use concentration in place of activity.

Minimizing drift and noise for a potentiometric sensor operating in a self-referencing mode (termed self referencing ion selective: SERIS [15]) can be explained by introducing a formulation of the Nernst equation. The voltage difference at the two poles of excursion within an ionic gradient is related to the concentrations at the two poles by the following equation:

$$\begin{aligned} E_1 - E_2 &= (E_0 + S \log C_{\mathrm{i}})_1 - (E_0 + S \log C_{\mathrm{i}})_2 \\ \Delta E &= (S \log C_{\mathrm{i}})_1 - (S \log C_{\mathrm{i}})_2 \\ \Delta E &= \log C_{\mathrm{i}(1)}^{S_1} - \log C_{\mathrm{i}(2)}^{S_2} \\ \Delta E &= \log \left(\frac{C_{\mathrm{i}(1)}^{S_1}}{C_{\mathrm{i}(2)}^{S_2}} \right) \end{aligned} \tag{18.3}$$

E_1 , $C_{\mathrm{i}(1)}$, and S_1 are the measured voltage, primary ion concentration, and slope of the voltage-log plot for the near pole of excursion. Subscript 2 labels the same parameters for the far pole of excursion. By calculating the difference in potentials over short periods of time the impact of slow drift, due to the constant potential differences throughout the system, are reduced. This places the emphasis of the potential difference measurement on the concentration difference of the ion.

Equation 18.3 can be simplified to determine the relationship between the ionic concentrations at the two points of excursion:

$$C_{\mathrm{i}(1)} = C_{\mathrm{i}(2)}^{S_2/S_1} \cdot 10^{\Delta E/S_1} \tag{18.4}$$

The slopes at two points of the calibration curve are included to address measurement of the primary ion under different circumstances; (1) differential concentration of the primary ion in the absence of an interfering ion; (2) differential concentration of the primary ion in a constant concentration of an interfering ion and; (3) differential concentration of a primary ion coexisting with a gradient of an interfering ion.

For an ideal electrode, used in the absence of interfering ions, the slope is constant over a wide range of the primary ion concentration and close to Nernstian. Under these conditions Equation 18.4 simplifies to:

$$C_{\mathrm{i}(1)} = C_{\mathrm{i}(2)} \cdot 10^{\Delta E/S} \tag{18.5}$$

Under many circumstances, the average concentration of the ion at the far pole, position 2, is not that different from the average concentration of the ion in the bulk solution. Therefore, the difference in ion concentration between the two points of excursion can be described as follows:

$$\Delta C = C_{\mathrm{i}(1)} - C_{\mathrm{i}(2)} = C_{\mathrm{bath}} 10^{\Delta E/S} - C_{\mathrm{bath}} \tag{18.6}$$

A primary assumption here is that the concentration difference measured between the two excursion points is linear. This is only true if the excursion distance is small compared to the extent that the gradient extends out into the bulk solution. For small cells an excursion of 10 μm will most likely sample over a distance in which the concentration difference is not linear and could, therefore, lead to an underestimate of the flux. An incorrect estimation of flux could also occur during a two-point measurement in an intense extended gradient, where the concentration of the ion at the far pole is substantially different from the background concentration of that ion. The solution to these issues is the use of a three-point measurement to; (1) more carefully map the concentration gradient with a third point to either ensure a linear relationship or determine a more accurate nonlinear relationship and; (2) to determine the concentrations in the gradient relative to the background concentration of the ion in the bath. For slow drift conditions, the electrode can simply be moved from position 3 (outside of the gradient) to position 2 (slightly into the gradient) to position 1 (deeper into the gradient). In general, regular measurements at all three positions should be attempted.

Measurement of a concentration difference for a primary ion in the presence of a constant concentration of an interfering ion presents us with a more difficult situation. Messerli et al. [14] have dealt with this in detail. Their results will be summarized here. Two variables in Equation 18.4 now need to be determined, specifically the concentration of the ion in the near pole $C_{\mathrm{i}(1)}$ and the new slope of the calibration curve in the near pole, S_1 . Therefore, a relationship between the change in voltage and the change in slope needs to be established in order to measure two points in a concentration gradient of a primary ion in the presence of a constant concentration of an interfering ion. The Nicolsky–Eisenman equation provides a means for predicting the change in slope due to the change in voltage in the presence of an interfering ion, assuming the electrode responds to the interfering ion in a Nernstian manner.

Rearranging the Nicolsky–Eisenman equation to get primary ion concentration in terms of voltage, we can determine the relationship of the slope at any point along the curve in terms of voltage:

$$\begin{aligned} E &= S_N \cdot \log\left(C_{\mathrm{i}} + K_{\mathrm{ij}} \cdot C_{\mathrm{j}}^{z_{\mathrm{i}}/z_{\mathrm{j}}}\right) \\ C_{\mathrm{i}} &= 10^{E/S_N} - K_{\mathrm{ij}} \cdot C_{\mathrm{j}}^{z_{\mathrm{i}}/z_{\mathrm{j}}} \\ \log(C_{\mathrm{i}}) &= \log\left(10^{E/S_N} - K_{\mathrm{ij}} \cdot C_{\mathrm{j}}^{z_{\mathrm{i}}/z_{\mathrm{j}}}\right) \\ \frac{1}{S} &= \frac{\mathrm{d}\log(C_{\mathrm{i}})}{\mathrm{d}E} = \frac{10^{E/S_N}}{S_N(10^{E/S_N} - K_{\mathrm{ij}} \cdot C_{\mathrm{j}}^{z_{\mathrm{i}}/z_{\mathrm{j}}})} \end{aligned} \tag{18.7}$$

S_N is 2.3 RT/z_{i} F and S is the slope along the curve. Z is the relevant valence and i is the measured ion and j the competing. In order to achieve this sort of measurement we need to know the starting position (voltage point) along the theoretical curve. One can calculate the starting voltage point on the theoretical curve by determining the slope in the bath empirically and solving for E in Equation 18.7.

$$E = S_N \log\left(\frac{S_N \cdot K_{\mathrm{ij}} \cdot C_{\mathrm{j}}^{z_{\mathrm{i}}/z_{\mathrm{j}}}}{S_N - S}\right) \tag{18.8}$$

The unknown S in the denominator is determined by calculating the slope between two different concentrations of the primary ion in the working solution. More points can be used to validate the starting position along the curve. From this point on the theoretical curve, a small change in measured voltage, ΔE , either up or down the curve, can be used to determine both the new slope at the near pole from Equation 18.7, and the concentration in the near pole from Equation 18.4. The differential concentration can now be determined as the concentration in the far pole and near pole are known.

The final case to be considered is measurement of a gradient of a primary ion coexisting with a gradient of an interfering ion. If a relatively ideal ISE can be used to measure the interfering ion then the situation discussed above with Equation 18.7 can be used to solve for the primary ion flux. However, if the ISE used to measure the interfering ion can also sense the primary ion then no simple electrochemical method to determine the absolute flux of either ion exists. Selective pharmacological block of targeted transporters can go some way to solving this problem by removing ion specific flux values. However, this is dependent on prior knowledge of the system.

Types of Potentiometric Ion-Selective Microelectrodes

Many more ISE designs, based on liquid membranes, exist than have been used in a self-referencing mode. Lists are available in Umezawa et al. [29] for inorganic cations, and Bühlmann et al. [30] with 30 available commercially from Sigma/Fluka. Calbiochem is another source. Fluka published data sheets for the ion selective solvents they offer [31]. As this publication is no longer generally available Table 18.1 gives the details for the ion-selective solvents that have been used in a self-referencing mode and unless stated otherwise this material comes from Fluka [31]. These data are also included to highlight the fact that all sensors are selective not specific. This critical point will be discussed below.

Not dealt with in Table 18.1 are interferents frequently used to block or activate molecular transport. This is a complex issue with no simple solution; examples are given for calcium detection [15] and for chloride detection [25,32]. Detecting a chloride flux over the actions of blockers or interferents is particularly interesting and has led to erroneous data getting into the literature [14,33,47]. The BioCurrents Research Center is compiling a web site database highlighting known problems (www.BioCurrents.edu) but any investigator is advised to conduct tests using their own system and solutions.

An interesting design for the detection of Cu fluxes has also been published [34]. As in Gow et al. self-referencing movement was manually controlled [10].

Choosing an Electrolyte

Before the front filling of the ISE with a column of ion-selective solvent, the micropipette is back filled with an electrolyte. The back filling solution is used to provide electrical contact between the back surface of the ion-selective solvent and the voltage-sensing node, via a Ag/AgCl wire. Usually a 100 mM solution of the ion being measured is used as the backfill to ensure that the ionic concentration between the back of the ion-selective solvent and the backfilling solution does not change significantly. However, it is now apparent that regulating this parameter can significantly alter the performance of the ISE.

Bakker and Meyerhoff review the phenomenon that the ion of interest from the back filling solution can easily move from the solution through the membrane into the bulk [28]. This will raise the local ion concentration effectively “blinding” the electrode to small activity changes at the tip. Clearly, there is a need to re-examine the use of more dilute solutions, and/or the use of ion buffers, in the electrolyte. Sokalski et al. show that the addition of buffer to the inner solution yielded picomolar detection levels for Pb^{2+} [35]. The influence of the electrolyte composition has also been demonstrated for K^+ detection using valinomycin [36]. Additionally, the backfilling solution should be matched osmotically to the bath solution. Osmotic gradients across the ion-selective solvent can lead to its movement into or out of the electrode tip, either causing the electrode to fail or an increase in noise (unpublished observation—Mark Messerli).

Self-Referencing: Amperometric Microelectrodes

Researchers have used amperometric electrodes in the self-referencing mode, taking advantage of the features discussed above for the potentiometric electrodes. To date all of the amperometric microelectrodes have been used in a constant potential mode. The electrode is clamped at a specific holding voltage to oxidize or reduce the analyte. This type of design and self-referencing application is termed self referencing potentiometric: SERP. Electrodes are built so that measurement of the analyte is limited by diffusion of the analyte itself, attempting to ensure a current dependent on the analyte concentration and not the concentration of a secondary factor or byproduct. The current generated by this redox reaction is, therefore, proportional to the concentration of the analyte. In the special case of enzyme-assisted electrodes (SERE) using glucose oxidase to measure a concentration difference of glucose, a by-product of the enzyme-substrate reaction, H_2O_2 , is measured [37].

For an ideal electrode under constant holding potential the measured current is proportional to the concentration of analyte. During self-referencing the differential current can be used to give a measurement of the differential analyte concentration:

$$\begin{aligned} I_1 - I_2 &= (I_0 + S \cdot C)_1 - (I_0 + S \cdot C)_2 \\ I_1 - I_2 &= S(C_1 - C_2) \\ \Delta C &= \frac{\Delta I}{S} \end{aligned} \tag{18.9}$$

I_1 and C_1 are the current and concentration of the analyte in the near pole of excursion. The subscript 2 has been used to identify the same parameters at the far pole of excursion. S is the slope of the calibration curve. Unlike ISEs, knowing the background concentration of the analyte is not necessary to determine the differential concentration due to the linearity of the current–concentration relationship.

Types of Amperometric Microelectrodes

The amperometric microelectrodes are solid-state, with a core of platinum, gold, or carbon as the electrolytic surface. The BRC has developed and published the application of Amperometric, and enzyme-assisted, self-referencing electrodes for the detection of oxygen, NO, hydrogen peroxide, ascorbate, glucose and glutamate [37–43]. Mancuso et al. independently published this approach for oxygen detection [44]. Oxygen electrodes produced by depositing thin layers of gold on optical fibers are also possible [20].

Calculation of Flux

To quantify the analyte movement in the bulk the differential concentration measurement is converted to flux. Not only does flux give a value proportional to transporter activity but it can also be used to calculate the total amount of analyte uptake or release by integrating the flux over space and time. Flux takes into account the diffusion coefficient of the analyte being measured, the distance over which the differential concentration measurement is acquired, the surface geometry of the source and the distance from the source. For cases where the measuring electrode is relatively close to a large source of the analyte and the differential concentration is measured over a small distance Δx within the gradient, the source can be modeled as a planar source so the flux (J) is:

$$J = -D\frac{\Delta C}{\Delta x} \tag{18.10}$$

where D is the diffusion coefficient of the measured analyte. By this model, the flux measured at some distance from the source is the same as the flux at the surface of the source. What constitutes a planar source? Kochian et al. found that the planar flux calculation is adequate for H^+ fluxes determined between a 30 μm distance, within 100 μm of a 1 mm diameter plant root [45]. However, for smaller cells or tissues, the geometry of the source must be taken into account [46,47].

In order to determine flux at the cell surface for known surface geometries it is useful to calculate analyte flow i.e., the quantity of substance (Q) moving per unit time [46]. Flow is the same for all concentric regions from the source surface. Flux at the source surface is the flow divided by the surface area of the source. Therefore, radially emanating flow from a cylindrical surface is:

$$\text{Flow} = \frac{Q}{t} = \frac{2\pi D}{\ln(b/a)}(\Delta C) \tag{18.11}$$

where D is the diffusion coefficient of the analyte and a and b are the radial distances between the center of the cylinder and the electrode tip at the near and far poles, respectively. Analyte flux at the surface of the cylinder is then determined by dividing by its surface area $2\varphi r^2$. A caveat to this approach is the assumption that the flow is equal at all points around the cylinder and along the shaft of the cylinder. An alternative is to calculate flux per unit length by dividing by $2\varphi r$ [46].

The flow from a spherical source is:

$$\text{Flow} = \frac{Q}{t} = 4\pi D \frac{ab}{b-a}(\Delta C) \quad 18.12$$

Flux at the cell surface can then be determined by dividing by the sphere surface area $4\varphi r^2$. These equations have been adapted from Crank [48].

A similar approach has been used in modeling a cluster of Hamster Insulinoma Tumor cells as an oblate spheroid to calculate the uptake of glucose [37]. The calculated glucose consumption per unit volume was 61.7 ± 9.5 fmol nl $^{-1}$ s $^{-1}$. This value is in close agreement with the results (48 fmol nl $^{-1}$ s $^{-1}$) using an absorption method and a mouse tumor cell line—EMT6/Ro [49].

Some researchers have chosen to forgo flux calculations as they are only interested in changes of the concentration measurement for cells and tissues under different conditions [50,51]. Given that the cells being used have relatively similar surface geometry, and that the electrodes are positioned at a similar position with respect to the cell surface, this simpler method is adequate.

Setting the Frequency and Distance of Translation

Unfortunately there is no simple rule concerning the selection of the correct translational frequency and excursion distance. These are influenced by the specific conditions of cells and electrodes. Put simply, an investigator should ensure that both poles of translation are within the gradient— preferably over a "linear" portion—and that the frequency is adjusted to allow a reasonable sampling period but one that avoids the impact of drift. The electrode must also have time to fully respond before data is collected. Messerli et al. deal with these matters in more depth [14]. Within the BRC default starting parameters of 0.3 Hz over a 10 µm translation are usually used.

Electrode Construction

Below are described the basic methods for making both potentiometric ion-selective solvent based electrodes and amperometric solid-state electrodes. With the correct apparatus, making ISEs is simple, applications being limited primarily by suitable ion selective cocktails (see above). Preparation of solid-state electrodes, at the dimensions and stability needed for self-referencing, is a different matter. The production of both metal and carbon core electrodes is tedious, with calibrations (see below) only indicating which electrodes *may* be useable in a self-referencing mode. Whereas, for example, an oxygen electrode calibrated by both dipping in solutions with different pO_2, or by cyclic voltammetry at different pO_2, can show a good DC response, the same electrode may prove too unstable or noisy for self-referencing applications. The basic electrode designs are shown in Figure 18.5, along with the reactive surface areas. Note that, simplistically, tip diameters do not represent reactive surface areas; it is the exposed area of the electrode that counts.

Electrode Construction: Potentiometric

The manufacturing of micron-sized ISEs used in biological systems has changed little in two decades and a detailed description of the process, as applied to self-referencing ISEs, is available [15]. Briefly, this method involves pulling borosilicate glass capillaries, without fibers, to the appropriate taper and tip size, 1–4 µm, using a Sutter P-97. 1.5 mm outer diameter, thin walled glass is normally used (World Precision Instruments TW150-4). The glass should be handled with non-powdered latex gloves. The pipettes are made in batches of around 50 and dried at > 200°C for at least 2 h. Hydrophobicity is produced by vapor silanization using *N* , *N* -dimethyltrimethylsilylamine (Sigma– Aldrich/Fluka cat # 41716). 50 µl is injected under the lip of glass beaker placed over the electrodes, standing vertically in a custom built rack (15 min: BioCurrents Research Center (BRC), Marine Biological Laboratory (MBL), Woods Hole, MA). Silanized pipettes can be stored for several days at 200°C or at room temperature in a container with desiccant.

Electrodes are made by backfilling the pipette with the appropriate electrolyte under slight positive pressure and then tip filling with the appropriate column length of ion-selective solvent from a micropipette reservoir (Table 18.2). The electrolyte column is kept short- ≈ 5 mm. This process is observed under the microscope and the two pipettes are aligned before applying pressure to backfill. It is particularly important that after backfilling, the tip is brought to the reservoir quickly or else the tip blocks [15]. Researchers choose the column length primarily for stability of the solvent in the pipette tip. For the examples given in Table 18.2, the H^+ and Ca^{2+} electrodes are made with a 30-µm column of solvent while the K^+ electrode is made with a 100–150 µm column length. This provides a more stable potassium electrode. Shorter lengths and the K^+ ion selective solvent is lost. The reason for these stability differences is probably the physical properties of the solvents used in the ion-selective cocktail.

The solvent used for H^+ (Sigma–Aldrich/Fluka cat #95293-1EA) and Ca^{2+} (Sigma–Aldrich/- Fluka cat # 21048-1EA) cocktails is *o*-nitrophenyl-*n* -octyl ether, which is 3.9 times more viscous, and nearly 3 orders of magnitude less soluble in water than 2,3-dimethyl-nitrobenzene [52]. The latter is used as the K^+ -selective solvent (Sigma–Aldrich/Fluka cat # 60398-1EA-F). There is certainly flexibility in the column length of the electrodes. ISEs are made fresh for each experiment.

A Ag/AgCl wire connects the electrolyte to the preamplifier via a standard electrode holder, available from several companies (for example Warner Instrument Corp: QSW-B15P). Clean silver wire is plated with chloride by passing 9 V, through the cathode via a 1 KΩ resistor, while immersed in a 1 *N* HCl solution. The process takes approximately 30 s. An Ag/AgCl reference electrode (MEH3815: World Precision Instr. Sarasota FL), connected via a 3 *M* KCl/5% agar bridge placed in the bulk solution, completes the circuit. The bridge is made with sodium acetate for experiments where K^+ ISEs are used.

ISEs should be calibrated in different concentrations of the targeted analyte made up in the physiological solution to be used in the experiment. A good practice is to use three concentrations, each an order of magnitude apart, that bracket the expected concentration in the saline to be used. For example, calcium might be used at 0.1 mM, 1.0 mM, and 10 mM. For H^+ sensors, unless there is a reason to expect problems from an unusual saline, calibration in commercially available buffer solutions are adequate provided a good pH value is determined on immersion in the saline at the start of the experiment. Under these conditions, the output from any ion selective solvent-based ISE should be close to Nernstian (see above). Extreme deviations indicate a failed electrode or the presence of a competing analyte in the saline to be used. Adding pharmacological compounds to these solutions is a simple and straightforward way to check for that type of interference. Garber et al. and Messerli et al. give good examples of this [14,32]. Electrodes should be calibrated before and after each experiment.

An additional calibration step is to compare the self-referenced output to a semi-empirical, modeled, gradient. Smith et al. explain this for the ISEs [15].

Electrode Construction: Amperometric

A number of solid-state amperometric microelectrode designs have been used in the self-referencing mode (Figure 18.5) and will be discussed below. A Ag/AgCl reference electrode, connected via a 3 *M* KCl/5% agar bridge placed in the bulk solution, completes the circuit. Reactive surface areas for the different designs are shown in Figure 18.5.

Making an Oxygen Electrode

Platinum wire, 25 μm in diameter, (1.5 cm length: Johnson Matthey, Ward Hill, MA) is straightened by rubbing with cardboard against a flat surface. These wires are then glued into 27 gauge hypodermic tubes (5 cm long: Small Parts, Inc., Miami Lakes, FL) with silver epoxy (Epoxy Technology, Inc., Billerica, MA) so that the Pt wire extends ≈ 1 cm from the tip. The wire is then electrochemically etched in an aqueous solution of 3 *M* KCN and 1 *M* NaOH by applying square waves of 4.0 V amplitude and a 4 ms period (pulse generator model 114 Tektronix, Inc., Portland, OR) until the tips are reduced to a fine point of < 1 μm. The etched Pt wires are rinsed with water and isopropyl alcohol and inserted into borosilicate glass capillaries (1B150, WPI) pulled to outer tip diameters of ≈ 3 μm using a Sutter P-97, so that the wire protrudes slightly from the pipette tip. The electrodes are dipped into epoxy (Epon 828 with *m*-phenylenediamine curing agent; Miller-Stephenson, Danbury, CT) and heated to 90±6°C on a hot plate. The electrodes dry overnight. At this stage the epoxy has sealed the Pt to the glass. A thin layer of epoxy probably coats the Pt protruding from the glass. Briefly dipping into acetone cleans the Pt. The epoxy is then cured by baking at 100°C for 2 h and 150°C for 2 h. The exposed Pt electrodes are etched again (same conditions as above) to form a recessed electrode with a cavity 2–3 μm deep. This etching takes no more than 5 min and can be monitored by examining the electrode under a microscope every 60 s. Finally, the electrodes are coated by dipping in a solution of 10% cellulose acetate (30 kDa: w/v in tetrahydrofuran, THF) for 60 s and drying for 10 min. In a more recent paper THF is replaced by acetone [37,53,54].

For oxygen detection, the electrodes are polarized to −0.6 V. Electrodes should be calibrated before and after each experiment by making measurements in nitrogen-bubbled (2–5 pA dark current) and normal air saturated salines (70 pA: 210 $\mu mol.l^{-1}$). When polarized incrementally from 0 to −1.0, the output in air-saturated saline should demonstrate a plateau between −0.6 and −0.8 V at ≈ 70 pA. Oxygen electrodes have a rapid response time (see below) and are normally used at a modulation frequency of 0.5–0.3 Hz over 10–20 μm. These parameters are, however, case specific. Land et al. present a measured versus a semi-empirically derived gradient [38].

Making a Hydrogen Peroxide Electrode

H_2O_2 microelectrodes are prepared as described above for oxygen sensors. The final tip diameter of the electrode is about 3 μm. The microelectrode is polarized to + 0.6 V against a Ag/AgCl reference electrode with a sensitivity of 0.85 ± 0.12 pA/μM (mean±SD, $n = 4$). Although the electrode can potentially detect other reactive oxygen intermediates beside H_2O_2 (such as NO and

O_2^-), in the applications cited, H_2O_2 is the major component of the concentration gradient, considering its longer half-life and the composition of the media (< 100 μM L-arginine) [40,41].

Making an Ascorbate Electrode

This involves sealing a 5 μm carbon fiber (Amoco, Greenville, SC) in a glass microcapillary. Heating and pulling the capillary draws it down to make contact with the fiber. The fiber is stabilized and sealed in the pulled glass pipette using epoxylite (Epoxylite Corp., Westerville, OH). After the epoxylite is cured in an oven at 110°C for 5–10 h, the electrode is backfilled with a graphite/epoxy paste (PX-grade Graphpoxy, Dylon Industries, Cleveland, OH). A copper wire can then be inserted to make electrical contact with the carbon fiber through the paste. The paste is cured (110°C for 5–10 h), and the excess carbon fiber chopped with a scalpel and beveled to 30° using a Narishige Model EG-44. This generates a comparatively large reactive surface area of ≈ 30 μm^2 . The electrodes are then electrochemically treated, based on previous studies. A 70 Hz triangle wave that cycles between + 3.0 V and + 1.5 V (7 s) is followed by a constant potential of + 1.5V (7 s), then held at 0.0 V for 30 min. The electrochemical treatment decreases the polarization voltage required for oxidation of ascorbic acid down to the 0.15–0.3 V range and delivers a reasonable selectivity for ascorbate under the conditions described by Pepperell et al. [42]

Experimentally the ascorbate microelectrodes have an applied voltage of 0.3 V, conferring good selectivity for ascorbic acid, and is oscillated over a distance of 30 μm at a frequency of 0.3 Hz [42].

Making a Nitric Oxide Electrode

The construction of the electrode body is the same as for the ascorbate electrode described above. To impart selectivity for the oxidation of NO, the carbon fibers are treated with Nafion and o-phenylenediamine (OPD) [55]. Nafion is a polysulfonated Teflon carrying an intrinsic negative charge that repels electrochemically active anions (e.g., nitrate, nitrite, and ascorbate). OPD is an electrochemically active material imparting a degree of selectivity for NO. The exposed carbon fiber surface is first coated with Nafion (5% in aliphatic alcohols, Aldrich cat #27,470-4) and dried at 110°C for 5–10 min. After two additional Nafion coatings, the fiber is plated using a 5 mM OPD plating solution containing 0.1 mM ascorbic acid in 100 mM PBS (pH 7.4). The OPD, prepared fresh for each use, is plated on the fiber at a constant + 0.9 V until a stable current is obtained [39].

The modified carbon fiber electrodes have final tip diameters of 7–8 μm, but after beveling have a reactive surface area of approximately 30–40 μm^2 , and are operated at + 0.90 V vs a Ag/AgCl return electrode, which completes the circuit in solution via a 3 *M* KCl/5% agar bridge. While the sensitivity of the NO electrodes for sodium nitrite is 1.43 ±0.16 pA/mM, the sensitivity for NO is 730 ±0.11 pA/mM [39]. Therefore, the NO electrodes are ≈ 500 times more sensitive to NO than nitrite.

NO electrodes can be calibrated with a standard 2 mM NO solution prepared by bubbling HEPES buffered saline with argon gas for 30 min and then compressed NO for 40 min in a fume hood. The saturation concentration of NO in aqueous media at 22°C is 2 mM (see Porterfield et al. 2001). Porterfield et al. present a comparison of the modeled versus measured NO gradient generated using the NO donor *S* -nitroso-*N* -acetylpenicillamine (SNAP). The modeling equation includes a correction for the ½ life of NO in an aqueous solution [39]. The electrode is operated at 0.3 Hz over a translational distance of 10 μm [39,56].

Making a Glucose (Enzyme-Assisted) Electrode

Glucose microsensors are fabricated in the first instance as described above for oxygen electrodes. The exposed Pt wires are etched to form a cavity ≈ 5 μm deep. Once etched, Pt particles are electrochemically plated on the recessed Pt wire at −0.2 V vs Ag/AgCl in a solution of 10 mM hydrogen hexachloroplatinate (IV) hydrate (Cat # 20,608-3: Aldrich, Milwaukee, Wisc.) for 3– 5 min. The amount of charge required for platinization is $1.2\pm0.3\times10^{-5}$ coulombs (mean±SD, $n = 26$). Glucose oxidase (GOx: EC 1.1.3.4, type X-S from *Aspergillus niger*: Sigma, St. Louis, MO) is then loaded onto the platinum particles by immersing the tip of the electrodes in 1% (w/v) GOx solution for 10 min. The enzyme is immobilized with 10% glutaraldehyde vapor for 1 min. The immobilized enzyme layer is then coated with 10%, 30 kD, cellulose acetate (w/v in acetone) by dipping (10 s) and drying (60 s), repeated 4 times. The final tip diameter is ~ 8 μm [37].

Calibration of the glucose electrode, polarized to + 0.6 V, is against 2, 5 and 10 mM glucose in 50 mM/l HEPES and 150 mM NaCl at pH 7.4 and 37°C. Experimentally the glucose electrode is operated at a frequency of 0.2 Hz over a 10 μm excursion. The speed of response to 90% is 0.46 s [37].

Making a Glutamate Electrode

Microelectrodes are fabricated in a manner similar to oxygen sensors, except that 8-μm carbon fiber, 12- μm gold wire, and 10- and 25- μm platinum wire were tested as a reactive surface. Electrodes were dip-coated with Os-gel-HRP redox polymer (BAS, W.

Lafayette, IN) and allowed to dry for 10 min. Electrodes were then dip-coated in 50 units/ml glutamate oxidase from *Streptomyces* sp. (Cat. # G-0400, Sigma) and allowed to dry for 10–30 min. Glutamate electrodes were polarized to either 0 or + 100 mV against a Ag/AgCl reference electrode, connected via a 3 M/l KCl/5% agar bridge placed in the bulk solution, to complete the circuit. The electrode was operated at a frequency of 0.1 Hz over a translational distance of 25 µm. The average response of platinum-based electrodes was 0.45 pA/µM of glutamate, whereas gold-based electrodes produce a weaker signal of 0.21 pA/µM, and carbon gave the weakest signal, 0.1 pA/µM. This electrode has not yet been used on a biological preparation [43].

Response Times

Sensor response times in rapidly changing flowing media frequently reveal values to 90% of the full response in the 10–100 ms range (see below and Table 18.2). These numbers are similar to some reports in the literature [57] but contradict others where response times in seconds have been reported [58,59]. As cited by Bakker et al. [27]—"Responses of ISEs can be so fast that the electronic equipment may become limiting ...." [52]. Similarly, millisecond response times for amperometric electrodes have been predicted by Schneiderman and Goldstick [60]. An increase in temperature can further decrease the response times of various ion selective sensor designs, an effect attributed to alteration in the diffusion coefficient or relative ionic mobilities [57].

Response time tests are conducted by changing the analyte activity in the bulk medium surrounding the microelectrode. To change solutions, work at the BRC uses an automated, parallel, flow-through system (Warner Instruments Corp.). This device allows three parallel streams of test solution to be passed over the sensor, with switching taking place in less than 10 ms for the complete movement. The microelectrode will see a faster event as it crosses the interface between the two streams. A manifold allows rapid changing of each stream to other solutions with minimal dead space. Using this system solutions of known composition, with or without potential interferents/toxins being present, can be passed over the reactive surface of the electrodes. Under these experimental conditions, the unstirred boundary layer at the bulk surface of the electrode will be minimal. This layer determines much of the limitation in response times for neutral carrier ISEs [27,61]. If electrodes are held stationary in a non-flowing analyte, this layer will be thicker.

Response Times: ISEs

Messerli et al. present data from response time testing on several ISEs (see Table 18.2) [14]. All fall in the millisecond range. Micron-sized, ISEs have high resistances; 1–20 G Ω [61]. Amplifier input impedances of 10^5–10^6 G Ω are typically used in conjunction with these electrodes to minimize current drawn and allow sampling of the ion concentration without significantly changing the local ion concentration. If the amplifier is ideal, what determines the speed of response for an ISE? Diffusion through the stagnant aqueous layer at the surface of the electrode defines the response time of the electrode when the membrane is equilibrated with the ion to which the electrode responds (Bakker et al. 1997). To put this in perspective consider the following theoretical analysis. If a system is diffusion limited, how quickly will an analyte diffuse from the edge to the center of the microelectrode? For a K^+ ISE, with a tip diameter of 4 µm, it would require only 0.3 ms ($t = L^2/6D_{K+}$ for diffusion in 3 dimensions, $D_{K+} = 2.0\times10^{-5}$ cm/s and L is the distance traveled). If the electrode were 1 mm in diameter, this diffusion to the center takes 21 s. All electrodes used with self-referencing have tip diameters of less than 10 µm and diffusion coefficients in the range of 10^{-4}–10^{-6} cm^2/s. Under these conditions the electronics will be the primary factor limiting the response time of the measurement under relatively ideal conditions.

Response Times: Amperometric

Tests using similar protocols to those described above also demonstrate relatively rapid response times for the amperometric electrodes (Table 18.2). Figure 18.6 gives an example for step change in the partial pressure of oxygen flowing past an O_2 electrode. The time to a 90% response is 17.95 ± 5.26 ms averaged for 4 electrodes. For a NO microelectrode (Figure 18.7) the values are 49.63 ± 13.21 ms averaged for 3 electrodes. Even the more complex glucose enzymeassisted electrode reaches 90% response in ≈ 500 ms (0.46 ± 0.07 s) [37].

Response Times: Interferents

As the self-referencing method requires that the electrodes remain stationary at the two poles for finite periods, any change to the response time is a source of concern. Such changes do occur. A 2– 3 µm K^+ -selective electrodes has a normal response time to 95% ($t_{95\%}$) of 41–77 ms depending on the change in concentration [14]. This ISE possesses $10^{3.9}$ selectivity for K^+ over Na^+, implying that a lot of Na^+ must be present to interfere with K^+ detection. However, animal salines can have significantly high levels of sodium. For example, in the presence of 450 mM Na^+ (seawater levels) the response time increases nearly 3-fold [14]. Further, the Nernstian response decreases by 8% [14]. Both of these features are classic indications of an interferent [27,62].

However, given that the data collected during the first 30% of the cycle time is discarded, the slower response time need not affect the data collected.

Spatial Resolution

Micron-sized electrodes provide good spatial resolution. For potentiometric electrodes the surface area of the ion-selective solvent in contact with the bulk medium defines this. The depth of sensing from the surface of a potentiometric electrode is considered negligible compared to the diameter of the ion-selective solvent interface, usually 1–4 μm. For example, if an electrode is being used to measure ionic concentration at a point near the surface of the cell, a 1–4 μm diameter electrode placed with the surface of the tip orthogonal to the cell surface will report the average concentration over the 1–4 μm tip diameter. Amperometric sensors used in constant potential mode, on the other hand, possess a sensing field that extends out into the medium away from the electrolytic surface. Take for example the O_2 -sensing electrode. The electrode generates current by reducing O_2 at its sensing surface. Reduction of O_2 consumes O_2 in the region immediately in front of the tip creating an O_2 depleted zone. These O_2 depleted fields have been modeled for both macro and microelectrodes with recessed and/or coated tips [60,63]. Carefully constructed electrodes, with recessed electrolytic surfaces and/or coatings, will limit the extent of this O_2 depleted field keeping the depletion zone restricted close to the tip. A well-constructed electrode can have virtually the entire O_2 depleted zone located within the recess at its tip. Therefore, the choice of design and construction of amperometric electrodes will have the greatest influence on defining the sensing zone.

Problems and Pitfalls

Potentiometric: Selectivity

It cannot be overemphasized that all the electrochemical techniques used in a self-referencing mode to date are selective not specific. There is always a finite chance that an interferent can be detected under experimental conditions designed for the primary analyte. As discussed above the differential approach inherent to self-referencing a microelectrode will greatly reduce the probability of simple background interferents being detected. However, unexpected problems can happen. Chloride detection using an ISE built with the Fluka Cl^- selective liquid ion exchanger cocktail A, is a good example. This ISE should more accurately be described as an anion sensor, even detecting a H^+ flux via sensitivity to the unprotonated anionic form of a Good buffer [14,47]. This ISE is also sensitive to a pharmacological agent used to block chloride transport, 4,4′-diisothiocyanatostilbene- 2, 2′-disulphonic acid (DIDS) [47]. Measurements of Cl^- with the more commonly used Cl^- ionophore I, cocktail A (Fluka Chemical Co) can sense or be poisoned by chloride channel blockers such as 5-nitro-2-(3-phenylpropyl-amino)-benzoic acid (NPPB), indanyloxyacetic acid 94 (IAA- 94), and DIDS [25,32].

Exposing an ISE to excitation light during imaging causes an additional area of interference. Hydrogen flux detection, while imaging the cytosolic pH sensor BCECF, is not possible with global illumination. In this case, the microelectrode couples to the excitation wavelength altering the Nernstian values and sensitivity (unpublished observation—Anthony Molina). Caged calcium has been released while using the amperometric oxygen microelectrode without adverse effect [64].

Amperometric: Selectivity

Amperometric electrodes are also susceptible to the detection of multiple molecules. For example, NO oxidation at a carbon fiber begins to plateau between + 0.8 and + 0.9 [65]. Neurotransmitters, ascorbic acid, nitrite and H_2O_2 can also be oxidized at this high voltage. A charged coating on the carbon fiber surface can eliminate passage of charged compounds [55,65]. However, H_2O_2 , an uncharged molecule, will be oxidized as it can pass through the coatings. Addition of a layer of catalase to the charged coating layers, similar to the enzyme layers used by Csöregi et al. [66] can eliminate H_2O_2 before it reaches the electrolytic surface.

Mixing

As self-referencing involves movement there is an inevitable risk of disrupting the gradient. This disruption can be minimal if a sufficient amount of time is allowed to pass for the gradient to be reestablished after sensor movement. The slow movement of the self-referencing microelectrodes, usually 40 μm/s, does not cause turbulence that can be detected visually. Also, the Reynolds numbers calculated for the speed of movement of either the small tip, 1–4 μm diameter, or even up the shaft where the diameter reaches 50 μm, are in the range of 10^{-4} to 10^{-3} , respectively, indicating that only laminar flow occurs around the tip of the electrode. However, in the worst-case scenario, if gradient disruption does occur how long must the microelectrode remain stationary for the gradient to be reestablished? If we consider the case of reestablishing the potassium gradient, after a 10 μm move between the near and far pole, we find that it will take about 8.3 ms for K^+ to diffuse this distance. This indicates that an ionic

gradient would be rebuilt in a few tens of milliseconds. As long as turbulent flow does not occur, most small analyte gradients will be rebuilt quickly.

Positional Artifacts

Positional artifacts can be broken into two types. The first concerns access or egress of analytes to or from the microelectrode tip. Specific cases are discussed below. The second potential artifact comes from a change in the geometrical relationship between the electrode and the target cell or tissue. By definition, the amplitude of a differential signal will depend on the position from the source and the recording position within the gradient. If this is not controlled then apparent flux changes will occur that actually represent a changing electrode to target distance. Although the motion controller design developed by the BRC shows exceptional stability [67], cells can move. This has constrained most studies to recordings made perpendicular to the visible edge of a cell or tissue, thus stabilizing distance by visual observation and software based manual adjustment.

Recently a new approach has been developed for the amperometric microelectrode that allows positional control through coupled electrochemical techniques [21]. In this case, an AC signal of 10 mV at 100 kHz is superimposed around the −0.6 V working potential of a self-referencing oxygen electrode. The monitored amplitude of this signal is dependent on the access resistance and, therefore, sensitive to the distance from an object. There is no interference between the two voltages and oxygen flux changes from a single INS-1 cell can be recorded while correcting for nanometer changes in electrode to target distance [21].

Positional Artifacts: Potentiometric

The positioning of ISEs near surfaces can generate artifacts. Of particular relevance to the selfreferencing technique is the possibility of ions emanating from the tip of the sensor and accumulating between the electrode tip and the target cell or tissue. The source of this potential artifact is a combination of current leakage from the electronics and zero-current (electroneutral) ion exchange of the primary ion for an interfering ion. This phenomenon has been shown for K^+ and Ca^{2+} - selective solvents [36,57]. The artifacts are most apparent in solutions of a low background primary ion. Reducing the concentration of the primary ion in the backfilling solution has been one compensation method [36]. Additionally, an applied current can control the flux across the membrane [57]. Pergel et al. used a current to compensate for the zero current phenomenon with Pb^{2+} detection [68]. None of these solutions have as yet been applied to self-referencing microelectrodes.

Positional Artifacts: Amperometric

In amperometric applications, the analyte is actually being consumed on the electrode surface. Therefore, an analyte depletion zone can form. An ideal electrode is built such that the analytedepleted region is located primarily within the electrode itself. However, it can quickly be envisioned that even a small depletion of the analyte in the bulk can give rise to a measurement artifact. In the extreme case, placing the electrode up against an insulator will prevent any analyte from reaching the surface of the electrode resulting in no change in current for a change in analyte. Backing the electrode away from the insulator, such that analyte can now diffuse, albeit in a restricted manner, will still give rise to a value below the real level. Moving back further, such that diffusion of analyte is not impeded, will result in maximal current for a change in analyte concentration. This phenomenon has been observed with the H_2O_2 product of the glucose electrode reaction building up between the electrode and a cluster of Hamster Insulinoma Tumor cells [54]. In that specific case, the artifact was removed by the addition of catalase to the medium.

Voltage Fields

In low conductivity medium, cellular currents can generate substantial voltage gradients next to the cells, coexisting with the chemical gradients of the analytes being measured. The potentiometric electrodes may sense these voltage gradients. Therefore, the voltage difference measured by the potentiometric electrode will be the sum of the voltage differences, due to the analyte concentration difference and the voltage difference, based on the current density and medium conductivity. In an animal system, however, the effect of voltage fields will be minimal due to the conductivity of the medium. Earlier studies using the vibrating voltage electrode confirm that these voltages are in the *n*V range and will not affect significantly the ISEs [18].

Static surface charges exist within the glycocalyx of cells because of molecular and ionic charge distribution. These charges will project their electrostatic effects into the bulk medium in accordance with the Debye length, 1/

. In the case of a mammalian Ringer, this is 7.8 Å (0.78 nm) [69]. All self-referencing microelectrode studies have been conducted at significantly greater distances.

Use of Buffers

There are a number of circumstances that cause the calculated flux to be smaller than measured. Buffering is clearly one of them. In the example discussed here, extracellular buffers can collapse gradients of free analytes. This has been addressed for the collapsing of H^+ gradients by H^+ buffers [33,70,71]. The analyte can diffuse from the surface of the cell in either its free state or bound to the buffer. ISEs only measure the free concentration of the analyte. The actual H^+ flux from a source is the sum of the measured free H^+ flux and the unmeasured H^+ flux moving as H^+ bound to buffer. The standard equations described above allow us to obtain the flux of H^+ ions through an unbuffered solution. It is, however, still possible to calculate a value, x_i , to represent the ratio of H^+ flux bound to buffer and H^+ unbound, a method recently applied to visual horizontal cells [70–72].

The ratio can be obtained using the equation:

$$x_i = \frac{D_{\mathrm{B}}}{D_{\mathrm{H}^+}} \cdot [\mathrm{B}] \cdot \frac{Ka}{(Ka + [\mathrm{H}^+])^2} \qquad 18.13$$

where D_{B} is the diffusion coefficient for protonated HEPES buffer (0.62×10^{-5} cm$^2 \cdot$ s^{-1}); $D_{\mathrm{H+}}$ is the diffusion coefficient for H^+ ions ($9.22\times10^{-5} \cdot$ cm^2 s^{-1}); and [B] is the buffer concentration in mol $\cdot$ cm^{-3} , which in experiments on the horizontal cells was 2.0×10^{-6} mol $\cdot$ cm^{-3} (that is, equivalent to 2.0×10^{-3} M), and the value for *Ka* (the dissociation constant for the buffer) is 3.16×10^{-11} mol $\cdot$ cm^{-3} [72]. Once the ratio is obtained, the total flux of H^+ can be calculated using the equation:

$$J_{\mathrm{Htotal}} = J_{\mathrm{Hmeasured}} + J_{\mathrm{Hbuffered}} = J_{\mathrm{Hmeasured}} \cdot (1 + x_{\mathrm{i}}) \qquad 18.14$$

That is, the total hydrogen ion flux from a cell is equal to the sum of the hydrogen ions detected by the sensor plus the hydrogen ions bound to buffer, which is not detectable, by the sensor. In order to minimize the effect of buffer on H^+ efflux a buffer with a *Ka*

below the [H^+] should be chosen, such that most of the buffer will be in its protonated form reducing the effective buffering capacity. The case of multiple buffers can also be considered [14,70].

In the absence of intentionally added H^+ buffers, water and dissolved carbonates can have a significant buffering effect at neutral to alkaline pH [70]. Water, at a concentration of about 56 M with a *Ka* of 10^{-16} begins to impact the correction factor above pH 6. The correction factor due to water acting as a H^+ buffer contributes to the total flux by less than 1% when the pH ≤ 6. Bicarbonate in solution, due to atmospheric CO_2 , will also have more significant impact at neutral to alkaline pH. Bicarbonate will increase in concentration at more alkaline pH, and can add to the H^+ flux by about 2 and 21% at pH 7 and 8 respectively [14].

Equipment and Software

The equipment and software described below are designed and assembled at the BioCurrents Research Center (Woods Hole, MA). All the development and microelectrode testing described above has been done using these designs. The basic components required to do self-referencing are the pre-amplifiers designed for potentiometric and amperometric detection, the main amplifier, a suitable PC with an analog to digital board, running the graphic user interface (GUI: IonView: Figure 18.2). This software also runs the motion controller interfacing with the 3-axis manipulator.

Preamplifiers

Voltage Head Stage Potentiometric

For potentiometric measurement the active element of the voltage head stage is an AD549 operational amplifier (op-amp: Analog Devices, Norwood, Ma.) configured as a voltage follower. This allows the microelectrode voltage to be sensed while drawing little current.

Current Head Stage-Amperometric

For amperometric measurements the components of the head stage are reconfigured to be a voltage clamp. The microelectrode is held at a command potential and the current that flows through the microelectrode is collected. An AD549 op-amp is configured as a current to voltage converter, having a 1 G Ω sense resistor. The command voltage is applied to the positive input of the op-amp and the microelectrode is attached to the negative input. An AD620 instrumentation amplifier is used to subtract the command voltage from the output of the op-amp leaving a voltage that is proportional to the microelectrodes current flow, times the value of the sense resistor, or 1 V per nA.

Amplifier

Amplification of the position dependant portion of the microelectrode signal must be sufficient for digitizing with reasonable resolution. The analog signal from the electrode must be amplified enough to make the sub-μV changes in voltage resolvable by the analog to digital converter without exceeding the dynamic range of the converter. Currently in use is a 16-bit data acquisition system (Datatranslation, Marlboro, MA) with a dynamic range of ± 10 V. This gives 65536 possible numbers to represent a voltage in the ± 10 V range, or 305 μV per least significant bit change. To resolve μV changes, a gain of 1000 times is applied, giving 305 nV per step or least significant bit change. The problem here is that the microelectrodes background voltage is frequently high, up to 100 mV. Since the dynamic range is ± 10 V the signal will have to be offset closer to zero volts before the gain is applied. Many methods can be used to do this. Two are currently in use at the BioCurrents Research Center. In the first a resistor and capacitor (RC), having a time constant of 10 s, generates a value that is subtracted from the non-filtered signal before the gain is applied, thus constructing a high pass filter. This allows signals faster than the time constant to be amplified while the impact of DC levels, and signals slower than the time constant, are minimized. The second method in use is a sample and hold approach. Here the computer, either by timed control or manual control (using a software button), sends a digital signal to a sample and hold component in the amplifier, latching the real time analog voltage to be the new reference or offset value of the live signal. Gain can be applied. In the above example the gain needed, and therefore the maximum offset that can be tolerated without exceeding the dynamic range of the analog to digital converter, is determined by the resolution of the converter (number of bits). If a high enough resolution converter becomes available, no nulling of the offset would be necessary.

Motion Control

Microelectrode movement is accomplished by a robotic manipulator and driving electronics. The system designed and used within the BRC comprises 0.9-degree stepper motors (Oriental Motors, Torrance, CA) fitted to Newport 433 and 432 translation stages (Newport Corporation, Irvine CA). The motors drive a 100 pitch lead screw via a zero backlash flexible bellows coupling

(Servometer, Cedar Grove, NJ). A motor, in turn, is driven by a 128 micro-step drive. Micro stepping increases the resolution of motion and smoothness of operation. The software increments or decrements the micro-step count to the motor and the shaft angle follows. Driving the motors with linear potential, rather than using the popular chopper method, reduces electrical interference but at the expense of motor torque. The system is capable up to several hundred microns per second at sub micron resolution and repeatability [67].

Software

IonView is the name given to the BRC windows program used for data acquisition and motion control. It has a standard graphic user interface (GUI). The current version of IonView provides simple access to data acquisition parameters-choice of RC subtract versus sample and hold, distance and speed of translation, and the choice of signal averaging. Data are processed and presented on screen, in real-time. As the polarity of the signal recorded is entirely dependent on which pole is subtracted from which, by convention one pole of translation is designated the + ve pole, as selected by the angle of movement, and is always the near pole of translation. A separate drop down window handles electrode positioning.

Applications

As the purpose of this paper is to introduce advances in a method, the many applications of selfreferencing to biological systems will not be reviewed. A collection of references to publications from the BRC, and others, can be found at the BRC web site (www.mbl.edu/BioCurrents). However, selected studies and publications, relevant to the neurosciences, are briefly introduced below.

Neural Repair and Disease

Microglia

These reactive cells of both vertebrate and invertebrate nervous systems have been the subjects of three studies using self-referencing microelectrodes. Chromogranin A (CGA) is a recently identified endogenous component of neurodegenerative plaques in Alzheimer's and Parkinson's diseases. CGA stimulates microglial secretion of NO and tumor necrosis factor-α, resulting in neuronal and microglial apoptosis. Using an electrochemical H_2O_2 microelectrode, it was demonstrated that CGA produces a rapid oxidative burst in primary microglia in culture [41].

Using both self-referencing K^+ and H^+ ISEs the presence of an K^+ /H^+ -ATPase in the microglia, with a K_D in the physiological range of the $[K^+]_0$, has been reported [50]. The pump was ouabain insensitive but modulated by Omeprazole and Sch28080. In this study, comparisons were also made between current values measured locally with an ISE and those calculated from whole cell patch clamp as related to the inward rectifying potassium channel. The ISEs followed ~ 0.5 of the whole cell current. Better signal processing methods developed since this study, and taking into account the problem of the electronics speed-of-response (discussed above), should now result in better correspondence to the total cell current.

In an invertebrate system, the leech, damage to the interganglionic connectives is hypothesized to stimulate the activity of eNOS, with the resultant production of NO causing the accumulation of migratory microglia at the lesion site. The production of the NO was measured directly from the lesion site using the electrode design discussed above [5].

Neural Tube Defects

One of the numerous complications of diabetes is the occurrence of embryonic congenital malformations, notably neural tube defects. Li et al. correlated this to the expression of Pax3 and tested the hypothesis that expression and embryopathy is related to a hypoxic state [73]. Hypoxia arises through diffusion limited oxygen delivery caused by excessive glucose metabolism. In this study, the selfreferencing oxygen microelectrode was used to demonstrate that embryonic oxygen consumption was suppressed after exposure to high maternal glucose levels. Along with other experiments, it was concluded that a depletion of oxygen in the embryo gives rise to impaired embryonic gene expression and defective development through induced oxidative stress [73].

Sensory Neurobiology

Hair Cells

The increase in K^+ flux through hair cells upon stimulation—whether by sound in the cochlea or acceleration in the vestibular labyrinth—is known to increase the perilymph $[K^+]$ on the basolateral side. Self-referencing K^+ ISEs, in conjunction with several other techniques, including micro- Ussing chambers, have followed these fluxes from both the strial marginal cells and the

vestibular dark cells [74–77]. In both tissues, the potassium channel responsible for the flux is the slowly activated K^+ channel (K_{sK}). The laboratories involved in this research have also made extensive use of the older vibrating voltage probe. This device has not been covered in this review. Interested parties are directed to Lee and Marcus for applications to the current studies in the ear and to Nuccitelli for an applications overview [78,18].

Hair cells of both the auditory and vestibular systems use calcium to control aspects of performance and tuning [79]. Self-referencing Ca^{2+} ISEs have been used to follow the role of the plasma membrane Ca^{2+} /H^+ ATPase (PMCA) in the regulation of this flux. A substantial calcium efflux could be measured, suggesting, in conjunction with pump density, that the PMCA activity should generate a substantial membrane current as the bundles expel cytosolic Ca^{2+} [79].

Vision

Horizontal cells isolated from the retina of the skate have provided a model system in vision research. Self-referencing hydrogen-selective ISEs have been applied to examine the relationship between glutamate and regional changes in extracellular pH [72]. The results suggested that glutamate modulation of H^+ flux arises from calcium entry into the cells and the subsequent activity of the plasma membrane Ca^{2+} /H^+ ATPase. The data from this reduced preparation did not support the action of hydrogen ions as part of an inhibitory feedback loop but further experiments are underway (R. Paul Malchow, unpublished).

Olfaction

Olfaction in estuarine animals, moving through different salinities, poses unique problems. To sample for chemical cues the sensillae must be exposed to changing osmotic and ionic conditions. Gleeson et al. used ISEs selective for K^+ and Ca^{2+} to question whether at low salinities the integrity of the olfactory dendrites of the Blue Crab are sustained by a diffusion generated ionic microenvironment within the aesthetascs [80,81]. Both ISEs confirmed this hypothesis with a clear loss of these ions from the hymolymph at low salinities. Further, the flux rates fell well within the range estimated from $^{22}Na^+$ flux data from previous studies [81].

Additional Electrically Active Cells

Neurons

Isolated neurons have been the subject of several self-referencing studies although limited by technical aspects of the technique. With the availability of positional control, as discussed above, and faster temporal resolution, one can anticipate more work on isolated neurons or networks, in addition to those mentioned above. Knox et al. in an early study of an isolated neuron, observed calcium influx and activation of a cation current, coupled to intracellular Ca^{2+} release, in peptidergic neurons of *Aplysia californica* [82]. Ca^{2+} released from a thapsigargin-sensitive store activated a non-selective cation current that may sustain depolarization of the somata. Using the same cell, Duthie et al. measured calcium fluxes in oxidatively challenged neurons [83]. Preliminary data on oxygen consumption, at the level of a single neuron, has been shown and correlated to membrane potential under voltage clamp conditions [84].

Muscle

Using self-referencing approaches on muscle are complicated by contraction. Contraction, particularly rapid contraction, will disturb the chemical gradient the microelectrodes are coupling to. However, under some conditions the technique can be successfully used, for example in muscle from the Sea Cucumber [85]. In this case Ca^{2+} flux changes were correlated with neurotransmitter application. Devlin also recorded Ca^{2+} flux modulation, to FMRFamide and 5-HT application, from the muscular trabeculae of the gastropod ventricle [86,87].

A mammalian muscular system studied with self-referencing is within the cerebral arteries. Membrane depolarization from −65 to −35mV is associated with myogenic contraction. Depolarization is graded to transmural pressure and sufficient to act on the open probability of the dihydropyridine-sensitive Ca^{2+} channel, augmenting the calcium contraction mechanism [25]. Using a self-referencing Cl^- ISE arterial Cl^- efflux can be measured with a clear temperature dependent pressure component that correlated closely to myogenic contractility [25]. This study concludes that Cl^- efflux, through Cl^- channels, contributes to the depolarization of the muscle cell. An additional attribute of this study is the realization that the ISE is affected by Cl^- channel blockers, such as DIDS, NPPB, and IAA-94. Pharmacological experiments are conducted using tamoxifen.

Amperometric detection has also been applied to L6 myotubes. Individuals suffering from type 2 diabetes mellitus have reduced expression of genes for key proteins in oxidative metabolism and mitochondrial function in muscle [88]. Measurements of glucose

oxidation from myotubes are unaltered by moderate overexpression of mitochondrial uncoupling protein 3 (UCP3) but markedly increased with the chemical uncoupler dinitrophenol (DNP). Glucose oxidation is measured using U-^{14}C Glucose and scintillation counting. This result is closely matched to the pattern of oxygen uptake monitored using self-referencing technologies. No difference in UCP3 expressing cells and control myotubes is found but a significant increase in oxygen uptake was seen with DNP treatment [88].

Pancreatic β-Cells

Pancreatic β-cells are the electrically active component of the Islets of Langerhans and secrete insulin in response to depolarization through voltage dependent Ca^{2+} channels. Part of the control pathway is the closure of the K_{ATP} channel regulated by changes in the ATP/ADP ratio as this relates to increased metabolism and circulating glucose levels. This predicts an oscillation in singlecell oxygen consumption at similar frequencies to insulin vesicle fusion. Porterfield et al. studying INS cells in culture, show this at the level of a single cell [89]. Damon Osbourn and Emma Heart have confirmed this observation on primary β-cell cultures and correlated activity with Ca^{2+} signaling (unpublished). Using INS cells, a method has been developed to simultaneous monitor oxygen flux with sub-micron spatial resolution of the microelectrode [21].

Additional Pumps and Channels

Apoptosis and Volume Changes

Apoptosis occurs in most cell types and can be triggered by a variety of physiological and pathological stimuli. It is a key mechanism in structuring tissues during development. This phenomenon has been studied using a mouse zygote (the condition prior to the first cleavage) and a selfreferencing K^+ ISE [51,90]. Cell shrinkage is an incipient hallmark of apoptosis and relates to changes in potassium flux that decrease the intracellular K^+ concentration, regulating apoptotic progression. This flux is measured at the single zygote level with apoptosis induced by H_2O_2 treatment [90]. Using a collection of pharmacological blockers for various K^+ channels, the mechanism underlying this change in K^+ flux is identified as the two-pore domain K^+ channel (K_{2P}) [51].

Ion fluxes, moving as a result of hyposmotic challenge and cell swelling, have been studied using single human epithelial tsA201a cells [32]. A role for an anion flux is critical in the induction of a recovery mechanism that ultimately involves the activation of voltage dependent potassium channels, a reduction in cytoplasmic osmolarity, and the initiation of flow of osmotically obligated water out of the cell. A clear chloride flux was followed using a self-referencing Cl^- ISE and was correlated to cell volume changes and membrane currents. This paper is of particular interest for the assessment of interferents to what would be better described as an anion selective ISE.

Acidification and Alkalinization

Self-referencing microelectrodes, although designed for applications to single or small groups of cells, can equally be applied to semi-intact epithelial structures. A series of papers studying the acidification of the vas deferens and epididymus of the rat is a good example [91–96]. The lumen of the mammalian vas deferens and epididymus is held at a pH of around 6.6, an important factor in the immobilization and maturation of sperm. Using a self-referencing H^+ ISE Breton et al. scanned the surface of the vas deferens locating hydrogen transport hotspots inhibited by Bafilomycin A1—a highly selective blocker for the vacuolar type proton ATPase (V-Type pump), a non-phosphorylating H^+ pump [91]. Subsequent studies have shown the involvement of chloride independent bicarbonate transport and an inhibition by cadmium [92,95]. Monitoring the localized H^+ flux has also allowed the study of the vesicle fusion event and a role for the cytoskeleton in trafficking and recycling of the V-Type pumps [93,96]. These studies have been conducted in conjunction with molecular and imaging techniques.

Using another epithelial structure, larval mosquito midgut, processes driving the extreme alkalinization of the anterior segment (pH≈ 11) have been studied with both H^+ and Cl^- selfreferencing ISEs [97,98]. Proton and chloride regional fluxes were mapped down the length of the midgut and pharmacological blockers used to determine their inter-relationship. Application of DIDS produced consistent results when measuring either H^+ or Cl^- flux. However, at 10^{-4}, M DIDS caused a small reversal of the Cl^- flux, a phenomenon not seen with methazolamide treatment [98]. This difference may be attributed to the interference of DIDS with the electrode performance as discussed above and by Messerli et al. [47]. The authors conclude that an H^+ V-Type ATPase energizes an anion exchange across the apical membrane. The electrophoretic Cl^- /HCO_3^- exchanger and carbonic anhydrase are seen as critical components in the alkalinization of the anterior midgut [98]. This study also presents an alternative approach to buffer correction when the diffusion coefficient of the buffer is unknown [98].

Conclusions

Electrochemical microelectrodes, whether stationary or self-referencing, offer unique advantages in studying the chemical composition of the cellular boundary layer. When operated in a self-referencing modulation mode these electrodes, both potentiometric and amperometric, follow the dynamics of chemical movement with high spatial and temporal fidelity. This format minimizes the impact of electrode and circuit drift, cuts out electrical boundary potentials, and chemical background signals. Being non-invasive, the approach further permits the tracking of changes from different locations over periods of seconds to days. Self-referencing microelectrodes, therefore, offer a powerful additional tool to an understanding of neuronal, glial, and cellular dynamics generally.

Acknowledgments

The authors would like to thank Robert Lewis for performing the response time studies, Tamara Clark for her graphics work, and our numerous collaborators, mentioned and unmentioned, for contributing so significantly to the further development of the techniques available at the BioCurrents Research Center. We also gratefully acknowledge the NIH: NCRR for funding the BRC as a national research resource (P41 RR001395 to PJSS).

References

1. Shou M, Smith AD, Shackman JG, Peris J, Kennedy RT. In vivo monitoring of amino acids by microdialysis sampling with on-line derivatization by naphthalene-2, 3-dicarboxyaldehyde and rapid micellar electrokinetic capillary chromatography. J Neurosci Methods. 2004;38:189–197. [PubMed: 15325127]
2. Sakmann B, Neher E. Single-Channel Recording. 2nd ed. Plenum Press; New York, London: 1995.
3. Inoué S, Spring KR. Video Microscopy: The Fundamentals. Plenum Press; New York: 1997.
4. Haugland RP. The Handbook—A Guide to Fluorescent Probes and Labeling Technologies. 10th ed. Invitrogen; Carlsbad, California, CA: 2005.
5. Travis ER, Wightman RM. Spatio-temporal resolution of exocytosis from individual cells. Annu Rev Biophys Biomol Struct. 1998;27:77–103. [PubMed: 9646863]
6. Pihel K, Hsieh S, Jorgenson JW, Wightman RM. Quantal corelease of histamine and 5-Hydroxytryptamine from mast cells and the effects of prior incubation. Biochemistry. 1998;37:1046–1052. [PubMed: 9454595]
7. Poitry S, Tsacopoulos M, Fein A, Cornwall MC. Kinetics of oxygen consumption and lightinduced changes of nucleotides in solitary rod photoreceptors. J Gen Physiol. 1996;108:75–87. [PMC free article: PMC2229314] [PubMed: 8854338]
8. Whalen WJ, Riley J, Nair P. A microelectrode for measuring intracellular PO_2. J Appl Physiol. 1967;23:798–801. [PubMed: 6061398]
9. Kang TM, Hilgemann DW. Multiple transport modes of the cardiac Na+ /Ca2+ exchanger. Nature. 2004;427:544–548. [PubMed: 14765196]
10. Gow NAR, Kropf DL, Harold FM. Growing hyphae of *Achlya bisexualis* generate a longitudinal pH gradient in the surrounding medium. J Gen Microbiol. 1984;130:2967–2974. [PubMed: 6527127]
11. Jaffe LF, Levy S. Proc IEEE/EMBS Conf. Vol. 9. 1987. Calcium gradients measured with a vibrating calcium-selective electrode; pp. 779–781.
12. Kühtreiber WM, Jaffe LF. Detection of extracellular calcium gradients with a calcium-specific vibrating electrode. J Cell Biol. 1990;110:1565–1573. [PMC free article: PMC2200169] [PubMed: 2335563]
13. Kang TM, Markin VS, Hilgemann DW. Ion fluxes in giant excised cardiac membrane patches detected and quantified with ion-selective microelectrodes. J Gen Physiol. 2003;121:325–347. [PMC free article: PMC2217369] [PubMed: 12668735]
14. Messerli MA, Robinson KR, Smith PJS. Plant Electrophysiology Theory and Methods. Springer; New York: 2006. Electrochemical sensor applications to the study of molecular physiology and analyte flux in plants.
15. Smith PJS, Hammar K, Porterfield DM, Sanger RH, Trimarchi JR. Self-referencing, non-invasive, ion selective electrode for single cell detection of trans-plasma membrane calcium flux. Micros Res Tech. 1999;46:398–417. [PubMed: 10504217]
16. Wipf DO, Bard AJ. Scanning electrochemical microscopy. 15. Improvements in imaging via tip-position modulation and lock-in detection. Anal Chem. 1992;64:1362–1367.
17. Siedlecki C, Marchant RE. Atomic force microscopy for characterization of the biomaterial interface. Biomaterials. 1998;19:441–454. [PubMed: 9677156]
18. Nuccitelli R. In Noninvasive Techniques in Cell Biology. Wiley-Liss; New York: 1990. Vibrating probe technique for studies of ion transport; pp. 273–310.
19. Kinlen PJ, Menon V, Ding Y. A mechanistic investigation of polyaniline corrosion protection using the scanning reference electrode technique. J Electrochemical Soc. 1999;146:3690–3695.
20. Smith PJS, Haydon PG, Hengstenberg A, Jung SK. Analysis of cellular boundary layers and their modulation by plasma membrane transporters: Application of electrochemical microsensors. Electrochim Acta. 2001;47:283–292.
21. Osbourn D, Sanger RH, Smith PJS. Determination of single cell oxygen consumption with impedance feedback for control of

sample-probe separation. Anal Chem. 77(21):6999–7004. [PubMed: 16255601]

22. Malchow RP, Land SC, Patel S, Smith PJS. Consumption of oxygen by isolated skate retinal photoreceptors measured using a self-referencing oxygen-selective microelectrode. Biol Bull. 1997;193:231–232. [PubMed: 28575613]
23. Smith PJS, Sanger RH, Jaffe LF. The vibrating Ca^{2+} electrode: A new technique for detecting plasma membrane regions of Ca^{2+} influx and efflux. In: Wilson L, Matsudaira P, Nuccitelli R, editors. Methods in Cell Biology A Practical Guide to the Study of Ca^{2+} in Living Cells. Vol. 40. Academic Press; San Diego: 1994. pp. 115–134. [PubMed: 8201973]
24. Smith PJS, Trimarchi JR. Noninvasive measurement of hydrogen and potassium ion flux from single cells and epithelial structures. Am J Physiol. 2001;280:C1–11. [PubMed: 11121371]
25. Doughty JM, Langton PD. Measurement of chloride flux associated with the myogenic response in rat cerebral arteries. J Physiol . 2001;534:753–761. [PMC free article: PMC2278745] [PubMed: 11483706]
26. Land SC, Collett A. Detection of Cl^{-} flux in the apical microenvironment of cultured foetal distal lung epithelial cells. J Exp Biol. 2001;204:785–795. [PubMed: 11171361]
27. Bakker E, Bühlmann P, Pretsch E. Carrier-based ion-selective electrodes and bulk optodes. 1. General characteristics. Chem Rev. 1997;97:3083–3132. [PubMed: 11851486]
28. Bakker E, Meyerhoff ME. Ionophore-based membrane electrodes: New analytical concepts and non-classical response mechanisms. Anal Chim Acta. 2000;416:121–137.
29. Umezawa Y, Bühlmann P, Umezawa K, Tohda K, Amemiya S. Potentiometric selectivity coefficients of ion-selective electrodes: Part 1. Inorganic cations. Pure Appl Chem. 2000;72:1851–2082.
30. Bühlmann P, Pretsch E, Bakker E. Carrier-based ion-selective electrodes and bulk optodes. 2. Ionophores for potentiometric and optical sensors. Chem Rev. 1998;98:1593–1687. [PubMed: 11848943]
31. Fluka. Selectophore, Ionophores for Ion-Selective Electrodes and Optrodes. Fluka Chemie A.G.; Ronkonkoma, New York: 1996.
32. Garber SS, Messerli MA, Hubert M, Lewis R, Hammar K, Indyk E, Smith PJS. Monitoring Cl^{-} movement in single cells exposed to hypotonic solution. J Memb Biol. 2005;203:101–110. [PubMed: 15981714]
33. Messerli MA, Danuser G, Robinson KR. Pulsatile fluxes of H^{+} , K^{+} , and Ca^{2+} lag growth pulses of *Lilium longiflorum* pollen tubes. J Cell Sci. 1999;112:1497–1509. [PubMed: 10212144]
34. Papeschi G, Mancuso S, Marras AM. Electrochemical behavior of a Cu/CuSe microelectrode and its application in detecting temporal and spatial localization of copper(II) fluxes along *Olea europaea* roots. J Solid State Electrochem. 2000;4:325–329.
35. Sokalski T, Ceresa A, Zwickl T, Pretsch E. Large improvement of the lower detection limit of ion-selective polymer membrane electrodes. J Am Chem Soc. 1997;119:11347–11348.
36. Mathison S, Bakker E. Effect of transmembrane electrolyte diffusion on the detection limit of carrier-based potentiometric ion sensors. Anal Chem. 1998;70:303–309.
37. Jung SK, Trimarchi JR, Sanger RH, Smith PJS. Development and application of a selfreferencing glucose microsensor for the measurement of glucose consumption by pancreatic β-cells. Anal Chem. 2001;73:3759–3767. [PubMed: 11510845]
38. Land SC, Porterfield DM, Sanger RH, Smith PJS. The self-referencing oxygenselective microelectrode: Detection of transmembrane oxygen flux from single cells. J Exp Biol. 1999;202:211–218. [PubMed: 9851909]
39. Porterfield DM, Laskin JD, Jung S.-K, Malchow RP, Billack B, Smith PJS, Heck DE. Proteins and lipids define the diffusional field of nitric oxide. Measurement of nitric oxide fluxes from macrophages using a self-referencing electrode. Am J Physiol. 2001;28:1, L904–912. [PubMed: 11557594]
40. Twig G, Jung SK, Messerli M, Smith PJS, Shirihai O. Real-time detection of reactive oxygen intermediates from single microglial cells. Biol Bull. 2001;201:261–262. [PubMed: 11687412]
41. Twig G, Graf SA, Messerli MA, Smith PJS, Yoo SH, Shirihai OS. Synergistic amplification of beta-amyloid and interferon-gamma-induced microglial neurotoxic response by the senile plaque component chromogranin A. Am J Physiol. 2005;28:8, C169–175. [PubMed: 15342341]
42. Pepperell JR, Porterfield DM, Keefe DL, Behrman HR, Smith PJS. Control of ascorbic acid efflux in rat luteal cells: Role of intracellular calcium and oxygen radicals. Am J Physiol. 2003;28:5, C642–651. [PubMed: 12724141]
43. Bogorff DJ, Messerli MA, Malchow RP, Smith PJ. Development and characterization of a self-referencing glutamate-selective micro biosensor. Biol Bull. 2003;205:207–208. [PubMed: 14583532]
44. Mancuso S, Paeschi G, Marras AM. A polarographic, oxygen-selective, vibrating-microelectrode system for the spatial and temporal characterization of transmembrane oxygen fluxes in plants. Planta. 2000;211:384–389. [PubMed: 10987557]
45. Kochian LV, Shaff JE, Kühtreiber WM, Jaffe LF, Lucas WJ. Use of an extracellular, ion-selective, vibrating microelectrode system for the quantification of K^{+} , H^{+} , and Ca^{2+} fluxes in maize roots and maize suspension cells. Planta. 1992;188:601–610. [PubMed: 24178395]
46. Henriksen GH, Raman DR, Walker LP, Spanswick RM. Measurement of net fluxes of ammonium and nitrate at the surface of barley roots using ion-selective microelectrodes. Plant Physiol. 1992;99:734–747. [PMC free article: PMC1080526] [PubMed:

16668947]
47. Messerli MA, Smith PJS, Lewis RC, Robinson KR. Chloride fluxes in lily pollen tubes: A critical reevaluation. Plant J. 2004;40:799–812. [PubMed: 15546362]
48. Crank J. The Mathematics of Diffusion. Oxford University Press; London: 1967.
49. Freyer JP, Sutherland RM. A reduction in the in situ rates of oxygen and glucose consumption of cells in EMT6/Ro spheroids during growth. J Cell Physiol. 1985;124:516–524. [PubMed: 4044662]
50. Shirihai O, Smith PJS, Hammar K, Dagan D. H^+ and K^+ gradient generated by microglia H/K ATPase. Glia. 1998;23:339–348. [PubMed: 9671964]
51. Trimarchi JR, Liu L, Smith PJS, Keefe DL. Apoptosis recruits two-pore domain potassium channels used for homeostatic volume regulation. Am J Physiol. 2002;28:2, C588–594. [PubMed: 11832344]
52. Ammann D. Ion-Selective Micro-Electrodes Principles, Design and Application. Springer-Verlag; Germany: 1986.
53. Jung SK, Kauri LM, Qian WJ, Kennedy RT. Correlated oscillations in glucose consumption, oxygen consumption, and intracellular free Ca^{2+} in single islets of Langerhans. J Biol Chem. 1999;275:6642–6650. [PubMed: 10692473]
54. Jung SK, Hammar K, Smith PJS. Development of self-referencing oxygen microsensor and its application to single HIT cells. Biol Bull. 2000;199:197–198. [PubMed: 11081733]
55. Friedemann MN, Robinson SW, Gerhardt GA. *O* -phenylendediamine-modified carbon fiber electrodes for the detection of nitric oxide. Anal Chem. 1996;1023:421–425. [PubMed: 8694261]
56. Kumar SM, Porterfield DM, Muller KJ, Smith PJ, Sahley CL. Nerve injury induces a rapid efflux of Nitric Oxide (NO) detected with a novel NO microsensor. J Neurosci. 2001;21:215–220. [PubMed: 11150338]
57. Lindner E, Gyurcsányi RE, Buck RP. Tailored transport through ion-selective membranes for improved detection limits and selectivity coefficients. Electroanalysis. 1999;11:695–702.
58. Mückenhoff K, Schreiber S, De Santis A, Okada Y, Scheid P. Ion-sensitive microelectrode system with short response time. J Neurosci Methods. 1994;51:147–153. [PubMed: 8051946]
59. Voipio J, Pasternak M, MacLeod K. Ion-sensitive microelectrodes. In: Ogden D, editor. Microelectrode Techniques The Plymouth Workshop Handbook. The Company of Biologists, Ltd; Cambridge, MA: 1994. pp. 275–316.
60. Schneiderman G, Goldstick TK. Oxygen fields induced by recessed and needle oxygen microelectrodes in homogenous media. Adv Exp Med Biol. 1976;75:9–16. [PubMed: 1015456]
61. Morf WE, Lindner E, Simon W. Theoretical treatment of the dynamic response of ion-selective membrane electrodes. Anal Chem. 1975;47:1596–1601.
62. Fleet B, Ryan TH, Brand MJD. Investigations of the factors affecting the response time of a calcium selective liquid membrane electrode. Anal Chem. 1974;46:12–15.
63. Schneiderman G, Goldstick TK. Oxygen electrode design criteria and performance characteristics: recessed cathode. J Appl Physiol. 1978;45:145–154. [PubMed: 670026]
64. Dumollard R, Hammar K, Porterfield M, Smith PJ, Cibert C, Rouviere C, Sardet C. Mitochondrial respiration and Ca^{2+} waves are linked during fertilization and meiosis completion. Development. 2003;130:683–692. [PubMed: 12505999]
65. Zhang X, Kislyak Y, Lin J, Dickson A, Coradosa L, Broderickand M, Fein H. Nanometer size electrode for nitric oxide and *S* -nitrosothiols measurement. Electrochem Commun. 2002;4:11–16.
66. Csöregi E, Quinn DCP, Schmidtke W, Lindquist SE, Pishko MV, Ye L, Katakis I, Hubbell JA, Heller A. Design, characterization, and one-point in vivo calibration of a subcutaneously implanted glucose electrode. Anal Chem. 1994;66:3131–3138. [PubMed: 7978306]
67. Danuser G. Photogrammetric calibration of a stereo light microscope. J Microsc. 1999;193:62–83. [PubMed: 12558688]
68. Pergel E, Gyurcsanyi RE, Toth K, Lindner E. Picomolar detection limits with currentpolarized Pb^{2+} ion-selective membranes. Anal Chem. 2001;73:4249–4253. [PubMed: 11569816]
69. Hille B. Ion channels and Excitable Membranes. 3rd ed. 2001. p. 342. Chap. 10.
70. Arif I, Newman IA. Proton efflux from oat coleoptile cells and exchange with wall calcium after IAA or fusicoccin treatment. Planta. 1993;189:377–383. [PubMed: 24178494]
71. Demarest JR, Morgan JLM. Effect of pH buffers on proton secretion from gastric oxyntic cells measured with vibrating ion-selective microelectrodes. Biol Bull. 1995;189:219–220. [PubMed: 8541412]
72. Molina AJ, Verzi MP, Birnbaum AD, Yamoah EN, Hammar K, Smith PJS, Malchow RP. Neurotransmitter modulation of extracellular H^+ fluxes from isolated retinal horizontal cells. J Physiol. 2004;560:639–657. [PMC free article: PMC1665295] [PubMed: 15272044]
73. Li R, Chase M, Jung SR, Smith PJS, Loeken MR. Hypoxic stress in diabetic pregnancy contributes to impaired embryo gene expression and defective development by inducing oxidative stress. Am J Physiol. 2005;28:9, E591–599. [PubMed: 15928021]
74. Wangemann P, Liu J, Marcus DC. Ion transport mechanisms responsible for K^+ secretion and the transepithelial voltage across

marginal cells of stria vacularis in vitro. Hearing Res. 1995;84:19–29. [PubMed: 7642451]

75. Marcus DC, Sunose H, Liu J, Bennett T, Shen Z, Scofield MA, Ryan AF. Protein kinase C mediates P_{2U} purinergic receptor inhibition of K^+ channel in apical membrane of strial marginal cells. Hearing Res. 1998;115:82–92. [PubMed: 9472737]
76. Marcus DC, Shipley AM. Potassium secretion by vestibular dark cell epithelium demonstrated by vibrating probe. Biophys J. 1994;66:1939–1942. [PMC free article: PMC1275919] [PubMed: 8075328]
77. Shen Z, Liu J, Marcus DC, Shiga N, Wangemann P. DIDS increases K^+ secretion through an IsK channel in apical membrane of vestibular dark cell epithelium of gerbil. J Membr Biol. 1995;146:283–291. [PubMed: 8568843]
78. Lee JH, Marcus DC. Endolymphatic sodium homeostasis by Reissner's membrane. Neuroscience. 2003;119:3–8. [PubMed: 12763062]
79. Yamoah EN, Lumpkin EH, Dumont RA, Smith PJS, Hudspeth AJ, Gillespie PG. Plasma-membrane Ca^{2+} -ATPase ensures low Ca^{2+} concentration in hair-cell stereocilia. Neurosci J. 1998;18:610–624. [PubMed: 9425003]
80. Gleeson RA, Hammar K, Smith PJS. Sustaining olfaction at low salinities: Mapping ion flux associated with the olfactory sensilla of the blue crab *Callinectes sapidus*. J Exp Biol. 2002;203:3145–3152. [PubMed: 11003825]
81. Gleeson RA, McDowell LM, Aldrich HC, Hammar K, Smith PJS. Sustaining olfaction at low salinities: evidence for a paracellular route of ion movement from the hemolymph to the sensillar lymph in the olfactory sensillar of the blue crab, *Callinectes sapidus*. Cell Tissue Res. 2000;301:423–431. [PubMed: 10994788]
82. Knox RJ, Kao LS, Jonas E, Connor J, Smith PJS, Kaczmarek LK. Calcium influx and activation of a cation current are coupled to an intracellular Ca^{2+} mobilization in peptidergic neurons. J Physiol. 1996;494:627–663. [PMC free article: PMC1160665] [PubMed: 8865062]
83. Duthie GG, Shipley A, Smith PJS. Use of a vibrating electrode to measure changes in calcium fluxes across the cell membranes of oxidatively challenged Aplysia nerve cells. Free Rad Res. 1994;20:307–313. [PubMed: 8069388]
84. Hammar K, Malchow RP, Smith PJS. Electrochemical measurement of O_2 consumption in single excitable cells. Biophys J. 2003;84:457A.
85. Devlin CL. A vibrating Ca^{2+} -selective electrode measures Ca^{2+} flux induced by the neuropeptide FMRFamide in a gastropod ventricle. Comp Biochem Physiol. 1997;116:93–100.
86. Devlin CL. 5-Hydroxytryptamine stimulates Ca^{2+} flux in the ventricular muscle of mollusk (Busycon canaliculatum) during cardioexcitation. Biol Bull. 2001;200:344–350. [PubMed: 11441976]
87. Devlin CL, Smith PJS. A non-invasive vibrating calcium-selective electrode measures acetylcholine-induced calcium flux across the sarcolemma of a smooth muscle. J Comp Physiol. 1996;166:270–277. [PubMed: 8810067]
88. MacLellan JD, Gowing A, Gerrits M, Smith PJS, Sivitz W, Wheeler MB, Harper MH. Increased uncoupling protein 3 stimulates fatty acid, but not glucose oxidation, and decreases reactive oxygen species in muscle cells. Diabetes. 2005;54(8):2343–2350. [PubMed: 16046300]
89. Porterfield DM, Corkey RF, Sanger RH, Tornheim K, Smith PJS, Corkey BE. Oxygen consumption oscillates in single clonal pancreatic β-cells (HIT). Diabetes. 2000;49:1511–1516. [PubMed: 10969835]
90. Trimarchi JR, Liu L, Smith PJS, Keefe DL. Non-invasive measurement of potassium efflux as an early indicator of cell death in mouse embryos. Biol Reprod. 2000;63:851–857. [PubMed: 10952931]
91. Breton S, Hammar K, Smith PJS, Brown D. Acidification of the male reproductive tract by bafilomycin-sensitive H^+ ATPase. Nat Med. 1996;2:470–472. [PubMed: 8597961]
92. Breton S, Hammar K, Smith PJS, Brown D. Proton secretion in the male reproductive tract: Involvement of chloride-independent bicarbonate transport. Am J Phyiol. 1998;27:5, C1134–1142. [PubMed: 9755067]
93. Breton S, Nsuma NN, Galli T, Smith PJS, Brown D. Tetanus toxin-mediated cleavage of cellubrevin impairs proton secretion in the male reproductive system. Am J Physiol. 2000;27:8, F717–725. [PubMed: 10807583]
94. Brown D, Smith PJS, Breton S. Role of V-ATPase rich cells in acidification of the male reproductive tract. J Exp Biol. 1997;200:257–262. [PubMed: 9050233]
95. Herak-Kramberger CM, Sabolic I, Blanusa M, Smith PJS, Brown D, Breton S. Cadmium inhibits vacuolar H^+ ATPase-mediated acidification in the rat epididymus. Biol Reprod. 2000;63:599–606. [PubMed: 10906070]
96. Beaulieu V, Da Silva N, Pastor-Soler N, Brown CR, Smith PJS, Brown D, Breton S. Modulation of the actin cytoskeleton via gelsolin regulates vacuolar H^+ ATPase (V-ATPase) recycling. J Biol Chem. 2005;280:8452–8463. [PubMed: 15591047]
97. Boudko D, Moroz L, Linser P, Trimarchi PJ, Smith P, Harvey W. In situ analysis of pH gradients in mosquito larvae using non-invasive, self-referencing, pH-sensitive microelectrodes. J Exp Biol. 2001;204:691–699. [PubMed: 11171351]
98. Boudko DY, Moroz LL, Harvey WR, Linser PJ. Alkalinization by chloride/bicarbonate pathway in larval mosquito midgut. Proc Natl Acad Sci. 2001;98:15354–15359. [PMC free article: PMC65033] [PubMed: 11742083]

Figures

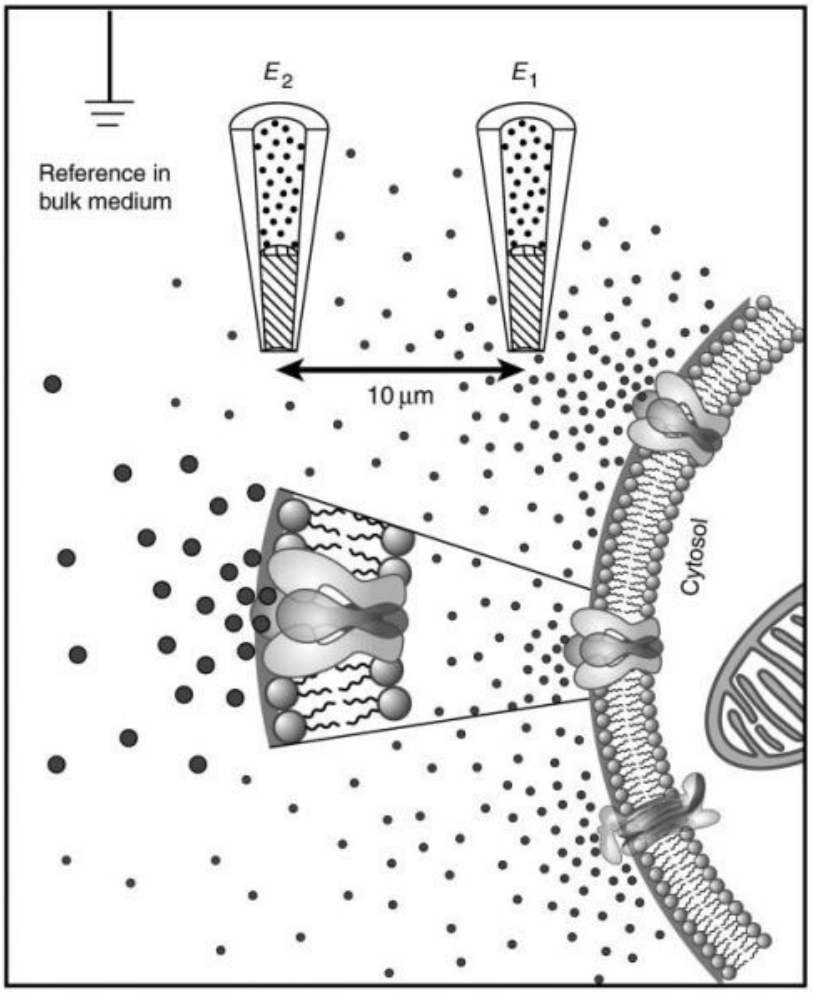

FIGURE 18.1

Self-referencing electrodes operate in the diffusive boundary layers surrounding cells and tissues. Within these layers, analytes form gradients depending on cellular activity, such as channel openings, as illustrated, or metabolism. This figure illustrates an ion-selective microelectrode located at both the near pole and far pole within an ion gradient. The voltages recorded, E 1 and E 2 , will depend on the activity of the ion. Comparing these two values generates a differential value minimizing the impact of non-relevant voltages generated by background levels of the analyte, junction potentials and competing analyte levels. The same principle applies to amperometric microelectrodes.

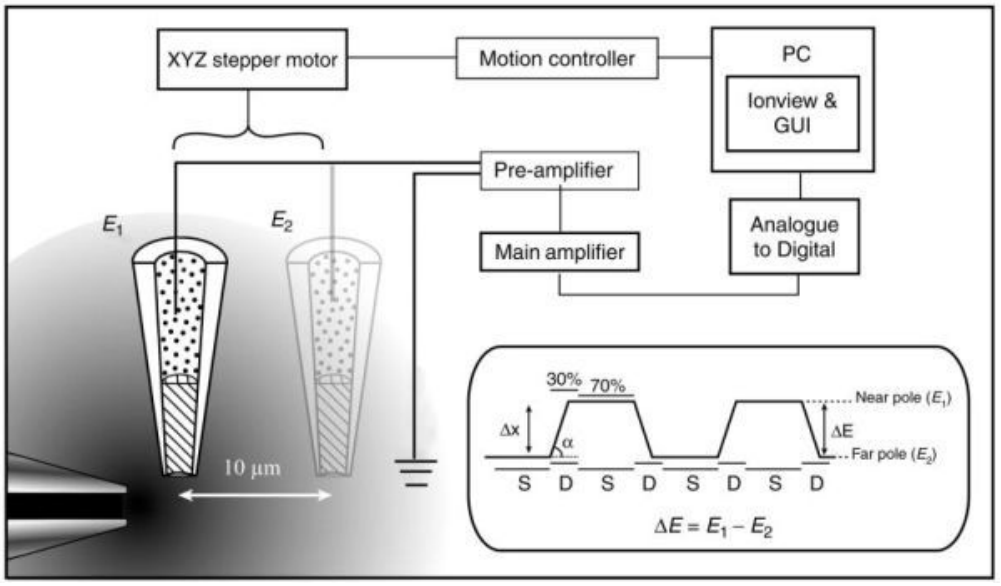

FIGURE 18.2

A schematic illustration of the self-referencing set-up. In this case a electrode is shown near a source of the analyte, moving in a "square" wave step between two positions 10 µm apart. Data is collected at 1000 points per second with the first 30% collected during and after translation being discarded (D). Movement is frequently set for a 10 µm displacement (Δ×) at a frequency of 0.3 Hz, thus data is collected at each pole for approximately 1 s or 70% of the cycle time (S). Comparing, in this case, voltages collected between the two extremes of movement, gives rise to a differential value (ΔE). A description of the electronics and software components are given in "Equipment and Software".

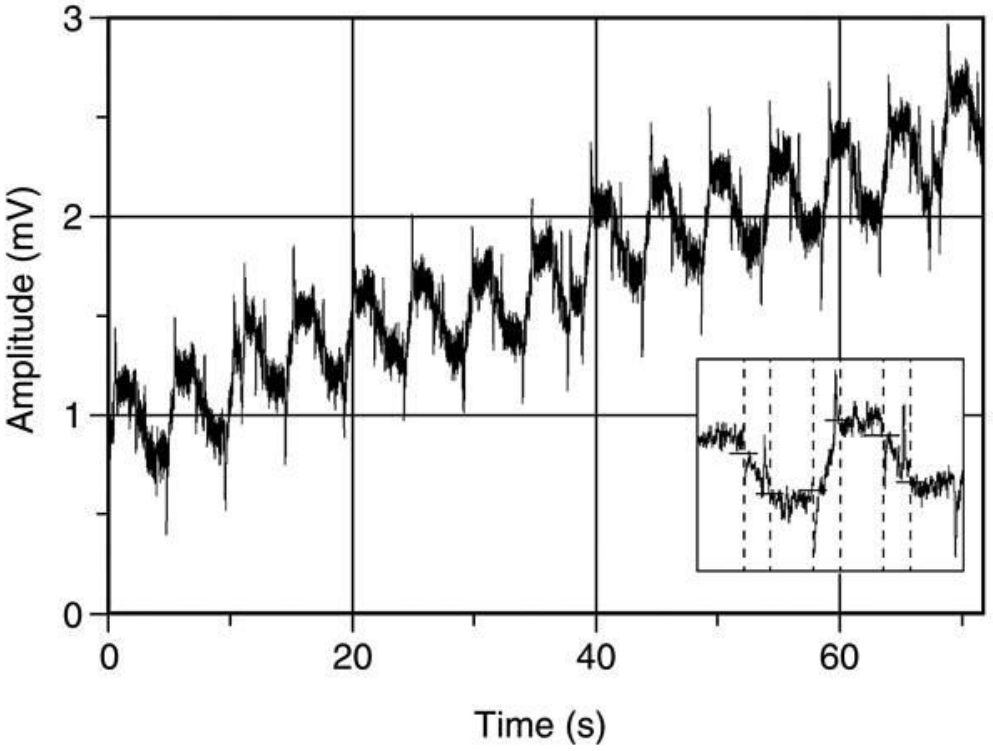

FIGURE 18.3

Raw data collected from a calcium ISE moving in a steep gradient generated by a 100 mM source of Calcium Chloride. A clear stepping of the data can be seen as the ISE moves between the two poles of translation. Significant drift in the base line is also evident. The insert shows the time scale for two cycles. The broken lines divide the signal into the discard and saved sections—see Figure 18.2. Biological signals will normally be in the microvolt range and therefore buried in the noise.

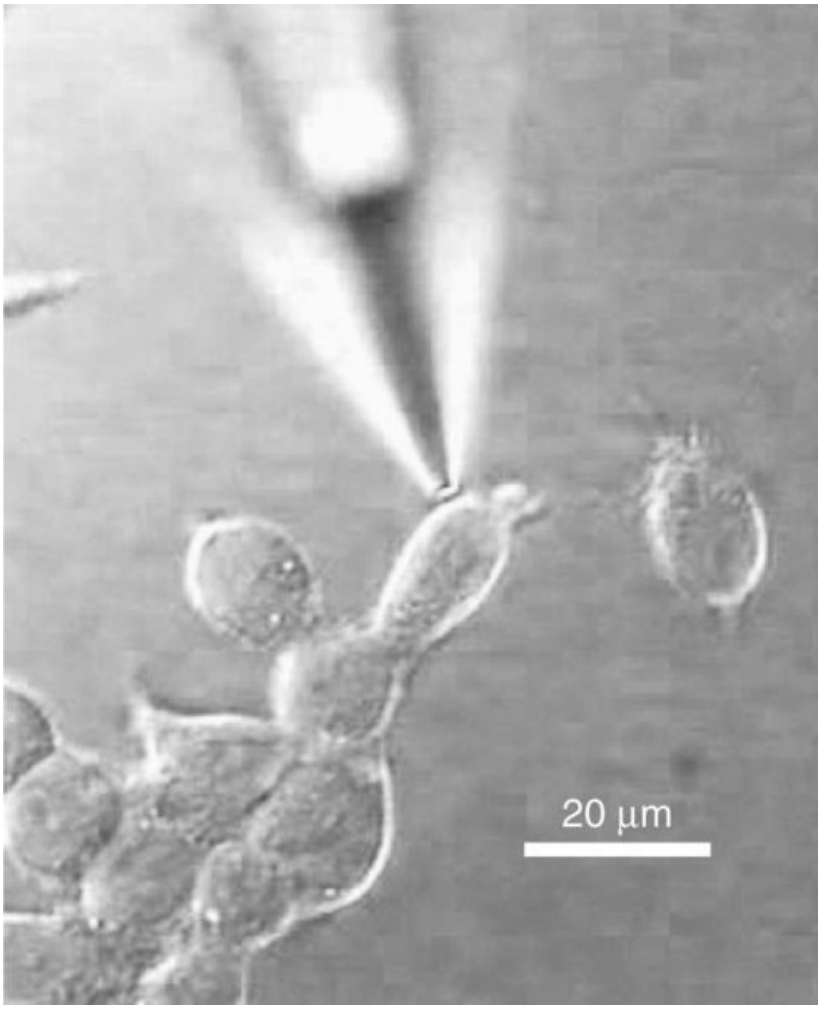

FIGURE 18.4

A real microelectrode near a real cell. This figure illustrates a Ca^{2+} ISE located at the near pole position for measurement from a cultured INS-1 cell. As the electrode is silanized, and the cocktail lipophilic, stability of electrode placement and movement is critical. The electrode must not touch the cell. Control of motion is discussed in “Equipment and Software”.

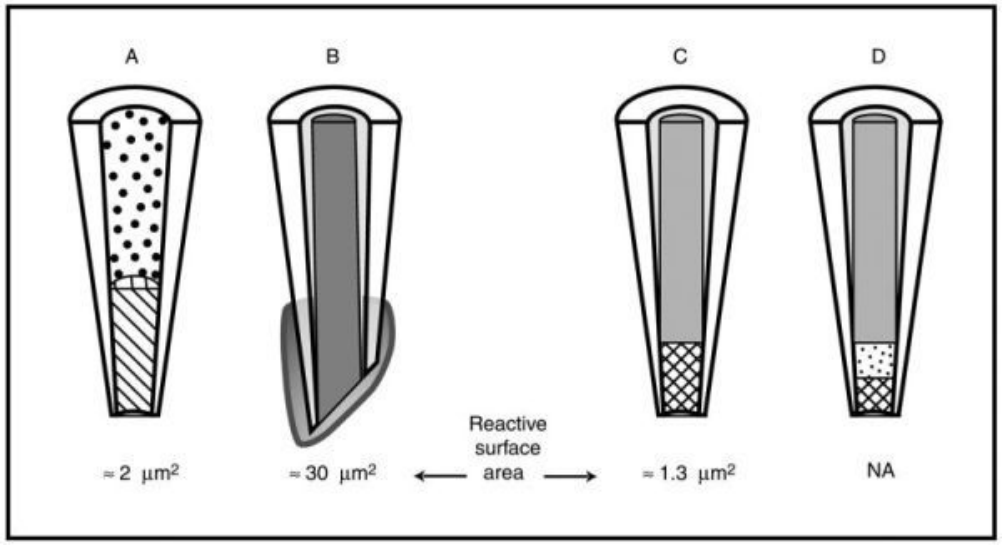

FIGURE 18.5

Diagrammatic representation of the potentiometric (A) and amperometric (B–D) electrode designs. In A, the electrode is made up of a pulled pipette backfilled with electrolyte and front filled with a short column of ion-selective solvent. Figure 18.4 shows a real example for the 30 µm column of Ca^{2+} selective solvent. The electrode design shown in B is a carbon fiber type as used for ascorbate and NO. The beveled tip has been coated with membranes to impart some degree of selectivity—see "Electrode Construction." The electrode types illustrated in C and D have a platinum core etched back to form a recess and closed with a cellulose acetate membrane. C is a design used for O2 detection. D has the recess prefilled with platinum spheres and an enzyme before capping. The latter design has been used for glucose detection. Electrode reactive surfaces are also given. These are approximate as tip diameters can vary.

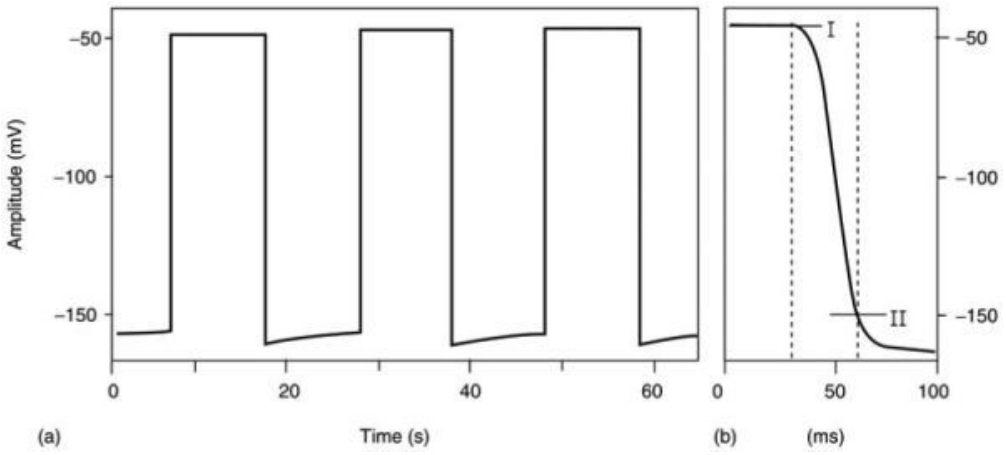

FIGURE 18.6

Speed of response for an amperometric Whelan-style oxygen electrode. Panel A gives examples of three exchanges between air equilibrated (more negative) and nitrogen bubbled. Panel B expands one exchange from low pO2 to air-saturated pO2 . Position I marks the beginning of the exchange to a new value and position II the arrival at 90% of the response. For this example this occurs in approximately 25 ms. These tests were conducted in a standard animal saline with 10 mM HEPES buffer-pH 7 saline.

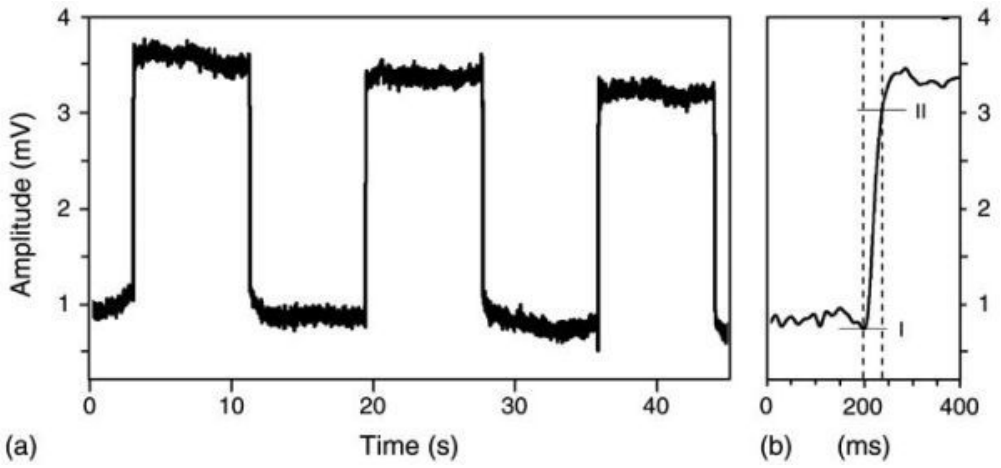

FIGURE 18.7

Speed of response for an amperometric nitric oxide electrode. Panel A gives examples of three exchanges between control and NO bubbled physiological saline. Panel B expands one exchange from control to NO bubbled. Position I marks the beginning of the exchange to a new value and position II the arrival at 90% of the response. For this example this occurs in approximately 50 ms. These tests were conducted in a standard animal saline with 10 mM HEPES buffer-pH 7 saline.

Tables

TABLE 18.1

Selectivities, Concentration-Dependent Slopes and Response Times for the LIXs Used in a Self-Referencing Mode

Calcium	
Fluka calcium ionophore I-Cocktail A. It has the following selectivity values determined by the fixed interference method:	
$\log K_{CaNa}^{Pot}$	−5.5
$\log K_{CaK}^{Pot}$	−5.4
$\log K_{CaMg}^{Pot}$	−4.9
Electrode function: Slope of the linear regression is 28.1 +/− 1.8mV (10^{-2} to10^{-7} $CaCl_2$ determined in calcium buffered solutions at a constant background of 125mM K^+). With a tip diameter between 1–2μm the expected resistance is in the range of 2×10^{10} Ω. Data from Fluka (1996). In our applications with larger tips(2–4μm) and short column lengths (30μm) we record a resistance of 2 3×10^{9} Ω . Response times evaluated at the BRC give a mean value of 48ms to 90% response (see below)	
Chloride	
Fluka chloride ionophore 1-Cocktail A. It has the followings electivity factors as determined by the separate solution method:	
$\log K_{ClHCO_3}^{Pot}$	−1.5[31]
	−0.9[32]
$\log K_{ClAcetate}^{Pot}$	−1.3[31]
	−1.2[32]
$\log K_{ClGlutamate}^{Pot}$	−3.2[32]
$\log K_{ClGlutamate}^{Pot}$	−3.0[32]
$\log K_{ClCitrate}^{Pot}$	−1.6[32]
$\log K_{ClThiosulfate}^{Pot}$	−0.8[32]
$\log K_{ClSO_4}^{Pot}$	−2.6[31]
$\log K_{ClSCN}^{Pot}$	3.4[31]
$\log K_{ClSalicylate}^{Pot}$	3.0[31]
Electrode function: Slope of the linear regression is 57.5+/−0.5 mV (0.001–0.5 *M* NaCl on 0.01*M* Tris/H_2SO_4, pH 7.4). The resistance for an approximately 1 μm tip will be in the region of 7×10^{10} Ω. These data are taken from [31]. The 90% response time is given as 1.8s [32]	
Hydrogen	
Fluka hydrogen ionophore 1-Cocktail B. It has the followings electivity factors determined by the fixed interference method:	
$\log K_{HNa}^{Pot}$	−10.4
$\log K_{HK}^{Pot}$	−9.8
$\log K_{HCa}^{Pot}$	< −11.1
Electrode function: Slope of the linear regression is 58.0+/−0.4mV pH range5.5–12.0. The resistance for an approximately1 μm tip will be in the region of 1×10^{11}Ω. These data are taken from [31]	
Response times evaluated at the BRC give a mean value of 88ms to90%.	
Potassium	
This cocktail has the following selectivity values based on the separate solution method:	
$\log K_{KLi}^{Pot}$	−4.2
$\log K_{KNa}^{Pot}$	−3.9

$\log K_{KMg}^{Pot}$	−4.6
$\log K_{KCa}^{Pot}$	−4.9
$\log K_{KAcetylcholine}^{Pot}$	−4.9
Electrode function: Slope of the linear regression is 58.8 +/− 1.2 mV (20°C:10^{-4} to10^{-1}). The detection limit of this ionophore is given as log a_K = −5.0 against 140 mM Na^+. These data are from [31]. The response time to 95% is 41 77 ms depending on the change in concentration [14]	
Cadmium	
These data are taken from Pineros et al. (1996). Reference should be made to this paper for ISE preparation and testing. Selectivity based on the separate solutions method:	
$\log K_{CdZn}^{Pot}$	−2.9
$\log K_{CsPb}^{Pot}$	−4.6
$\log K_{CdCu}^{Pot}$	−4.8
$\log K_{CdMn}^{Pot}$	−5.2
$\log K_{CdFe}^{Pot}$	−8.6
$\log K_{CdNi}^{Pot}$	−10.4
$\log K_{CdCa}^{Pot}$	−10.8
$\log K_{CdMg}^{Pot}$	−12.2
$\log K_{CdNH_4}^{Pot}$	−6.2
$\log K_{CsNa}^{Pot}$	−7.1
$\log K_{CdK}^{Pot}$	−7.9

TABLE 18.2

Characteristics and Response Times Determined for a Variety of Electrochemical Micro-sensors under Different Conditions. All Tip Diameters and Reactive Areas Are Approximate

Electrode	Column Length	Tip Size	Medium	Response Times (t_{95}% ms)for Concentration Ranges			
				10 1mM	1 0.1mM	0.1 1mM	1 10mM
K^+	100 µm	1 µm	1	195±59	376±86	165±41	114±26
	1000 µm	1 µm	1	369±91	516±86	247±54	191±46
	100 µm	2 3 µm	1	41±3	77±4	53±4	44±3
	100 µm	2 3 µm	2	64±9	225±6	91±8	69±15
				pH 6 7	pH 7 8	pH 8 7	pH 7 6
H^+	30 µm	1 µm	3	209±12	220±15	214±27	202±13
	300 µm	1 µm	3	251±21	269±14	245±11	244±17
	30 µm	2 3 µm	3	135±23	130±32	126±30	124±35
				10 1mM	1 0.1mM	0.1 1mM	1 10mM
Ca^{2+}	30 µm		4	58±9	81±10	48±7	53±10

Electrode			Surface Area	Medium	Response Times (t_{90}% ms) to Different Partial Pressures.	
					Air—N_2 saturated	$N_{saturated}$ Air
O_2	n.a.		2 μm^2	4	17.95±5.26	17.03±5.75
					Saline—NO bubbled	NO bubbled—Saline
NO	n.a.		30–40 μm^2	4	49.63±13.21	61.00±14.33

Medium 1.100mM HEPES (pH 7.0) with 0.1, 1.0 or 10 mM KCl Medium 2. Medium 1 with 450 mM NaCl Medium 3. 100 mM MES (pH 6), 100 mM HEPES (pH 7,8)set with KOH Medium 4.InmM, 120NaCl,5 KCl,2 $CaCl_2$, 2$MgCl_2$ 10 HEPES (pH 7.4).

Bookshelf ID: NBK2573 PMID: 21204387